Available online at www.sciencedirect.com
ScienceDirect
Journal of Sound and Vibration 300 (2007) 522–551
JOURNAL OF SOUND AND VIBRATION
www.elsevier.com/locate/jsvi

Nonlinear energy pumping under transient forcing with strongly nonlinear coupling: Theoretical and experimental results

E. Gourdon[a,*], N.A. Alexander[a], C.A. Taylor[a], C.H. Lamarque[b], S. Pernot[b]

[a]*Department of Civil Engineering, University of Bristol, Queen's Building, University Walk, Bristol BS8 1TR, UK*
[b]*Ecole Nationale des Travaux Publics de l'Etat, LGM, URA CNRS 1652, Rue Maurice Audin, F-69518 Vaulx en Velin Cedex, France*

Received 5 December 2005; received in revised form 27 April 2006; accepted 13 June 2006
Available online 20 October 2006

Abstract

This paper aims to experimentally verify the theoretical effects of energy pumping especially with external excitation. Energy pumping is irreversible transfer of energy from a linear or linearized structure to a nonlinear energy sink (NES) with relatively small mass. This NES can be used as a nonlinear absorber. This phenomenon is analyzed for different kinds of excitation. In suitable range of amplitudes of the external forcing, the damped system exhibits quasiperiodic vibrational regime rather than periodic responses reported in earlier publications. This regime can be explained by using nonlinear normal mode theory. Mechanical experiments confirm the theoretical results by using a small building model. In particular, the case of earthquake excitations is investigated.

1. Introduction

Conventional vibration absorption devices, used in Civil Engineering, are linear and require the addition of significant mass to the structure. Designers of structures, which may be subject to earthquakes, commonly seek to reduce the total structural mass. Thus, it is important to develop new absorption devices that reduce both stationary and transient responses while adding as little extra mass to the structure as possible. Moreover, it is interesting to design new devices being able to absorb vibrations for a broad spectrum of frequency. This is particularly important for the case of seismically forced systems that are not subject to monochromatic inputs. Nonlinear passive absorbers can be designed with far smaller additional masses than linear absorbers. They make use of the energy pumping phenomenon which has been studied recently [1,2]. This latter corresponds to a controlled one-way channeling [3] of the vibrational energy to a passive nonlinear structure where it localizes and diminishes in time due to damping dissipation [4,5]. So nonlinear energy pumping can be used in coupled mechanical oscillators [6] where the essential nonlinearity of the attached absorber enables it to resonate with any of the linearized modes of the substructure [2]. A nonlocalized nonlinear normal mode is thus introduced with strong oscillations in the second added structure far from the main structure to be isolated and with very small oscillations in the first structure. So, through energy

*Corresponding author. Tel.: +33 4 72 04 77 46; fax: +33 4 72 04 70 41.
E-mail address: gourdon@entpe.fr (E. Gourdon).

0022-460X/$ - see front matter © 2006 Elsevier Ltd. All rights reserved.
doi:10.1016/j.jsv.2006.06.074

pumping, vibrations of a forced linear structure (subjected to an external excitation) can be attenuated with the help of nonlinear coupling. Energy pumping can be used during earthquakes, where transient dynamics are important. Numerical examples of the latter point are presented in Ref. [7].

In this paper, a nonlinear passive absorber, i.e. an energy sink, is attached to a linear primary structure. The additional mass is connected solely to the top of the linear, or linearized, primary structure. This is an example of a real application for vibration absorption in tall buildings. This paper aims to experimentally verify the efficiency of employing the nonlinear energy pumping phenomenon in the case of building vibrations.

To this end, an idealized simple building model, where only the fundamental sway mode is considered, was designed, built and tested in Earthquake Laboratory of University of Bristol, UK. Damping and natural frequency parameters of the idealized simple building model were chosen to be in the range of typical real low rise buildings.

The outline of the paper is as follows. In the next section, the experimental and numerical considered systems are introduced. In the third section, analytical and numerical studies are presented to show the possible behavior of such a structure. The fourth section is devoted to experimental verification by using different transient excitations.

2. System considered

By employing modal analysis the fundamental sway mode can be represented by an equivalent linear oscillator. Thus, the analytical system consists of this linear oscillator, for the simple building structure, and a strongly nonlinear coupled oscillator, for the nonlinear passive absorber (with a small mass). The nonlinear terms are cubic in nature. The system excitation is either harmonic or transient in nature, i.e. an earthquake motion.

The experimental system is shown in Fig. 1 and represented in Fig. 2. The secondary mass, of the absorber, can slide along an aluminium roller guide rails fixed to the top of the simple building. $x_1(t)$ and $x_2(t)$ represent

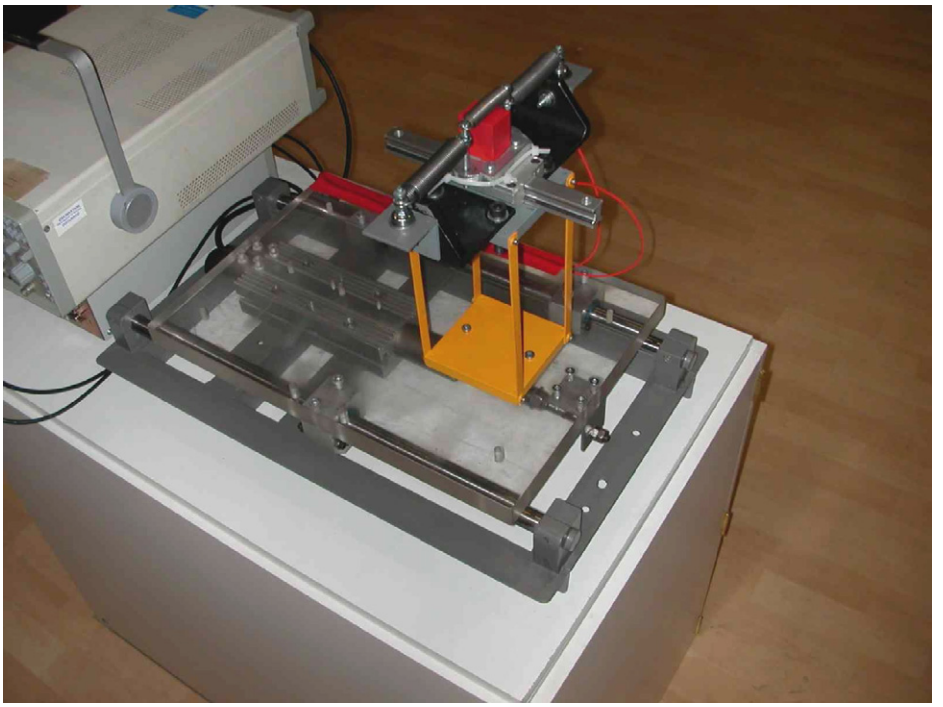

Fig. 1. Experimental system.

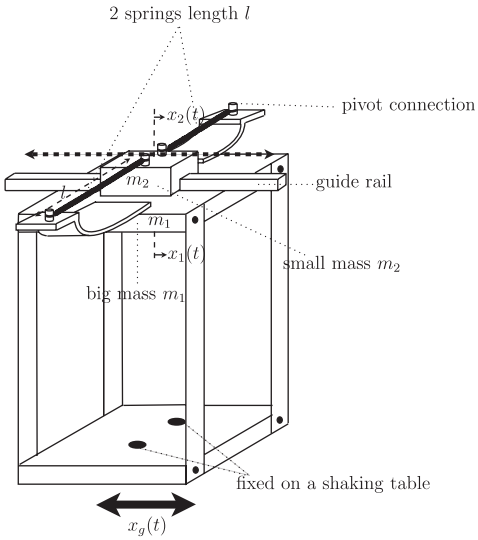

Fig. 2. Considered system with 2 dof.

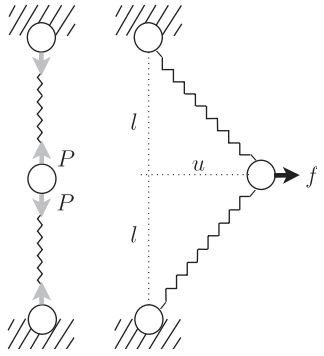

Fig. 3. Design of the cubic nonlinearity.

absolute displacements of the primary mass and of the secondary mass, respectively. $x_g(t)$ is the displacement of the structural supports. For pragmatic experimental reasons, it is easier to employ absolute coordinates rather than relative ones. m_1 denotes the mass of the primary structure and m_2 the mass of the second added structure. In this experiment, the idealized viscous damping coefficient between the primary mass and the supports is c_1 and between the primary mass and the secondary mass is c_2.

The supports of the simple building model are connected to a small-scale uni-axial shaking table. This table was designed, built and tested at the Earthquake Laboratory of University of Bristol. Table itself is driven by a computer controlled Linmot actuator (Linmot E1000 MT controller characterized by the ability to efficiently stream almost any excitation profile: sine dwells, sine sweeps, random noises, pulses, earthquakes,...) which horizontally moves the table along linear ball bearing guide rails. As underlined in Ref. [8] the cubic nonlinearity can be implemented geometrically with two linear springs. Thus, the nonlinearity is experimentally implemented with two linear springs (k and l are, respectively, the stiffness and the length of one linear spring) as shown in Fig. 3. The linear springs extend axially and are free to rotate about their supports. Flexural behavior of the springs induced by inertial actions is neglected. The stiffness force $F(u)$—displacement u relationship is given by the following equation (1) which is approximately cubic in nature with the help of a Taylor series expansion (where P is pre-stress force in the

springs and $|u| \ll 1$).

$$f = 2ku + \frac{2u(P-kl)}{\sqrt{l^2+u^2}} \approx \frac{2P}{l}u + \frac{kl-P}{l^3}u^3 + O(u^5). \tag{1}$$

However, as underlined in Ref. [8] when the pre-stress force P is approximately zero, the linear terms of Eq. (1) can be neglected. Experimentally P must be kept to a minimum. The springs have been calibrated by measuring the deflection under a static load. By using a variety of different spring sizes it is possible to adjust the coefficient in front of the cubic nonlinearity. Experimental derived values for $F(u)$ versus u are plotted in Fig. 4 and are fitted by using a nonlinear least square optimization procedure to identify the nonlinear characteristic.

It should be underlined that the cubic approximation in Eq. (1) has been widely used in such problems and then the equations are easier to manipulate since theoretical analysis (with analytical expressions) is easier and possible. However, in numerical simulations, since Runge–Kutta schemes are adopted, we will use the exact expression. We will comment the relative error which is very small when we will use the cubic approximation.

Thus, the building and nonlinear absorber can be idealized by the model displayed in Fig. 5. The complete system is given by the following equations:

$$\begin{cases} m_1\ddot{x}_1 + c_1\dot{x}_1 + k_1x_1 + c_2(\dot{x}_1 - \dot{x}_2) + k_2(x_1 - x_2)^3 = k_1x_g + c_1\dot{x}_g, \\ m_2\ddot{x}_2 + c_2(\dot{x}_2 - \dot{x}_1) + k_2(x_2 - x_1)^3 = 0, \end{cases} \tag{2}$$

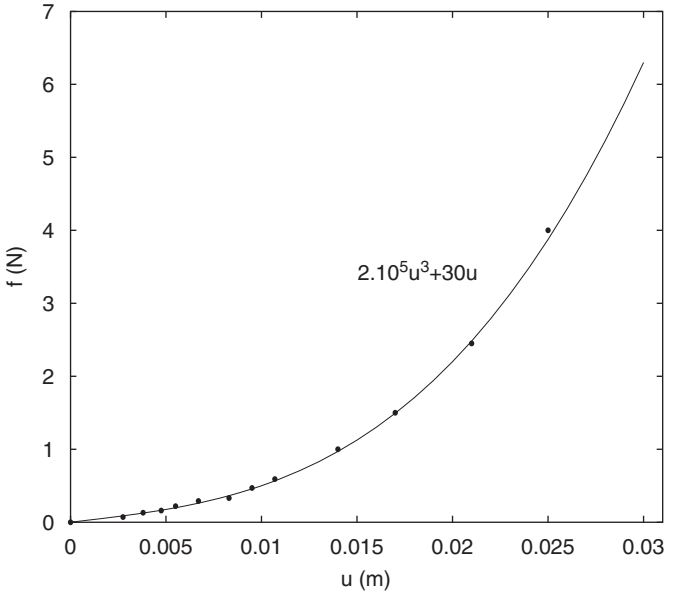

Fig. 4. Force–displacement characteristic of the nonlinear spring. The dots correspond to experimental results and the line corresponds to a cubic fitting.

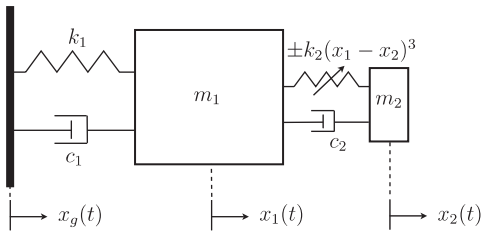

Fig. 5. Scheme of the considered system with 2 dof.

where $k_2 = k/l^2$. By defining $\varepsilon = m_2/m_1$ ($\varepsilon \ll 1$) and $\omega_1^2 = k_1/m_1$, $\lambda_1 = c_1/m_2$ $\lambda_2 = c_2/m_2$, $\omega_2^2 = k_2/m_2$, then:

$$\begin{cases} \ddot{x}_1 + \varepsilon\lambda_1\dot{x}_1 + \varepsilon\lambda_2(\dot{x}_1 - \dot{x}_2) + \omega_1^2 x_1 + \varepsilon\omega_2^2(x_1 - x_2)^3 = \omega_1^2 x_g + \varepsilon\lambda_1\dot{x}_g, \\ \varepsilon\ddot{x}_2 + \varepsilon\lambda_2(\dot{x}_2 - \dot{x}_1) + \varepsilon\omega_2^2(x_2 - x_1)^3 = 0. \end{cases} \tag{3}$$

Two PCB piezotronics accelerometers, with a good sensitivity at low frequencies, have been attached to the structure (Fig. 1). One is connected under the plate of the primary mass and the other one is connected above the secondary mass. Modal identification is performed by a pole-residual technique using Matlab structural dynamic toolbox SDTools.

The experimental parameters are $m_2 = 0.33\,\text{kg}$, $m_1 = 3.3\,\text{kg}$ so $\varepsilon = 0.1$. A modal analysis and experimental dynamic analysis of the structures give $\omega_1 = 29.2\,\text{rad}\,\text{s}^{-1}$, $c_1 = 1.4\,\text{N}\,\text{s}\,\text{m}^{-1}$, $c_2 = 5\,\text{N}\,\text{s}\,\text{m}^{-1}$ and $\omega_2^2 = 6.06\times 10^5\,\text{N}\,\text{m}^{-3}\,\text{kg}^{-1}$. Thus $\lambda_1 = 4.24$ and $\lambda_2 = 15.15$. So the specific natural damping for the linear primary structure ($= c_1/2m_1\omega_1$) is 0.73% and the specific natural damping for the second added structure ($= c_2/2m_2\omega_2$) is 0.97% (Fig. 5).

The natural frequency of the primary structure, without the absorber, is 4.65 Hz and is an approximated value for the fundamental natural frequency of a two-storey building.

The use of the cubic approximation is justified here as shown in Fig. 6 where the exact expression in Eq. (1) and the cubic approximation have been compared owing to numerical simulation (with a Runge–Kutta

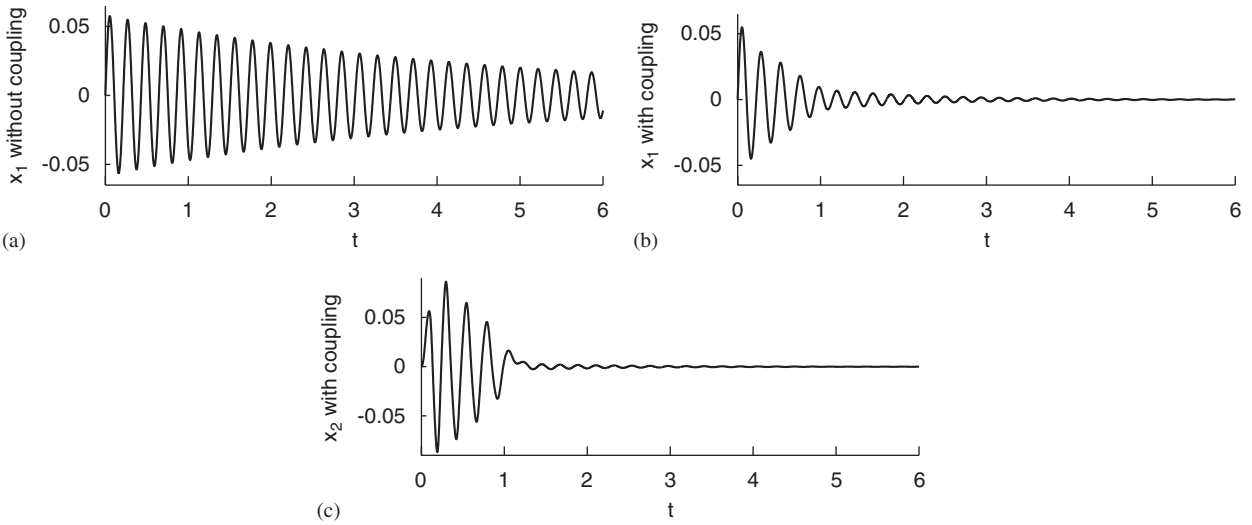

Fig. 6. Evaluation of the cubic approximation in Eq. (1): the solid line denotes the exact solution and the dotted line denotes the approximation: (a) x_1 with no coupling; (b) x_1 with coupling; and (c) x_2 with coupling.

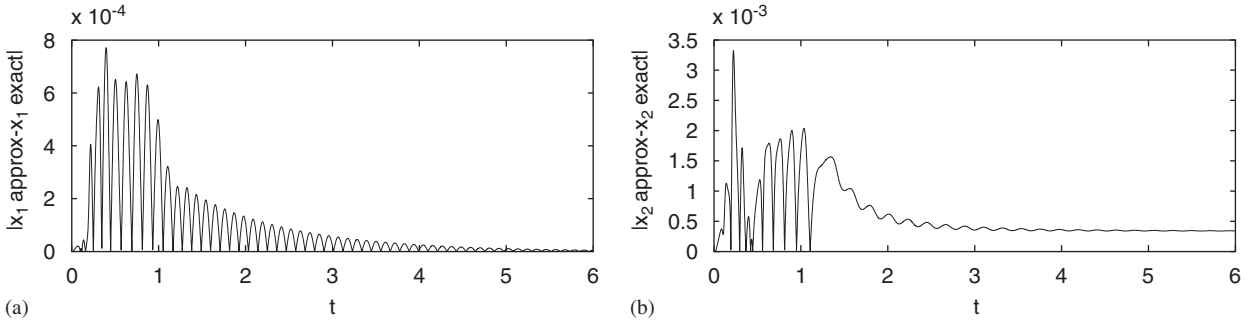

Fig. 7. Evaluation of the relative error by using the cubic approximation in Eq. (1): (a)$|x_1\text{approx} - x_1\text{exact}|$; (b) $|x_2\text{approx} - x_2\text{exact}|$.

scheme). The values of parameters are the same as mentioned previously (with $k = 780\,\mathrm{M\,m^{-1}}$, $l = 0.109\,\mathrm{m}$, $x_1(0) = x_2(0) = \dot{x}_20 = 0$, $\dot{x}_10 = 1.2$). The two cases are quasi identical. We can also compare the relative error as shown in Fig. 7 which is very small when the cubic approximation is used. The maximum of the error is 7.71×10^{-4} for x_1 and 3.32×10^{-3} for x_2. The error is smaller for x_1 since the cubic approximation is less important in the equation of motion of the first mass.

3. Theoretical analysis and numerical study

First, impulsions with free oscillations are considered. By means of appropriately designed electric circuit as shown in Fig. 8, previous Eqs. (2), (3) can be analyzed; such experiment allows to estimate the robustness of energy pumping as the electric circuit inevitably contains additional damping and other factors not accounted in the analytic and numerical models. As shown in Fig. 9, energy transfer from the directly excited linear oscillator to the unexcited nonlinear oscillator takes place with attenuation of oscillations of the linear structure and resonance of the second nonlinear oscillator with the same frequency (which defined a 1:1 resonance). Secondly, pure harmonic forcing $x_g = G\cos(\omega t)$ is considered. Let $\omega = \omega_1 = 29.2\,\mathrm{rad\,s^{-1}}$; thus the dynamics of the system are analyzed in the vicinity of the most dangerous resonance. The frequency of the external excitation is hence the natural frequency of the linear oscillator. Numerical simulations, using a Runge–Kutta scheme, show the quasiperiodic vibrational regime of the damped system in Fig. 10 where $\omega_1^2 G = 2.5\,\mathrm{m\,s^{-2}}$. To confirm that this solution is quasiperiodic and not periodic, the Poincaré's sections for the two oscillators are shown in Fig. 11. Here, *the Hénon trick* is used. The Poincaré application is defined by

$$P(x_{i0}) = x_i(x_{i0}, t_0; t_0 + T), \quad i = 1, 2, \tag{4}$$

where x_{i0} are the solution of initial system (2) which go through the point x_{i0} at time $t = t_0$ and $T = 2\pi/\omega$. The points x_{i0}, $x_{i1} = P(x_{i0})$, $x_{i2} = P^2(x_{i0}), \ldots$ correspond to the intersection of the trajectory $x_i(x_{i0}, t_0; t)$ with the planes $t = t_0$, $t_0 + T$, $t_0 + 2T, \ldots$, respectively. Those points form a sequence of stroboscopic images of the solution at regular time intervals $\Delta t = T$ [9].

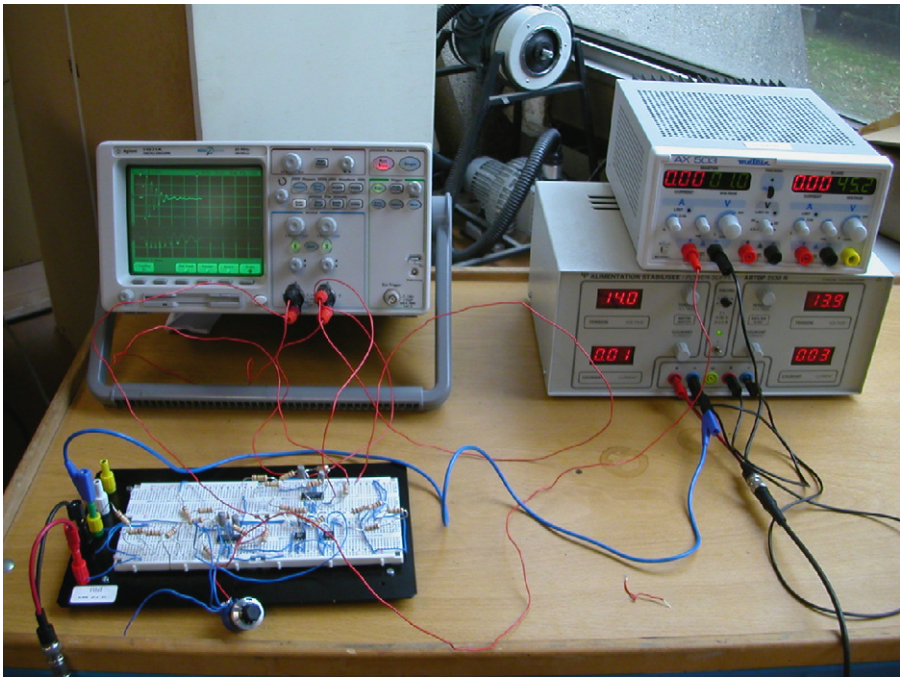

Fig. 8. Considered system with 2 dof by means of electric circuit.

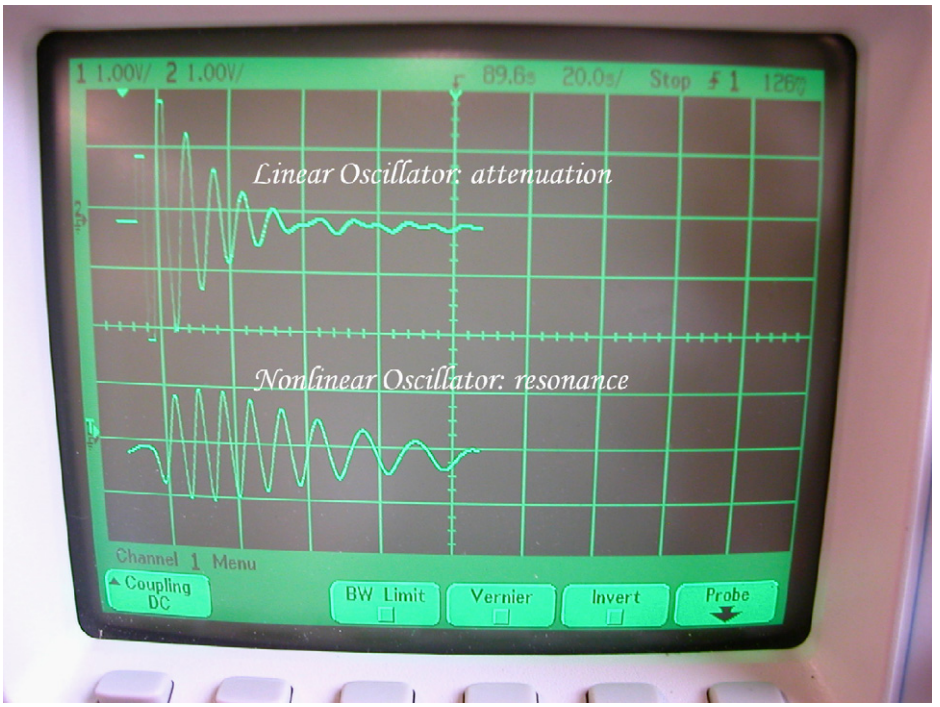

Fig. 9. Results obtained by means of electric circuit.

One possible application of this proposed nonlinear absorber is related to absorption of vibrations in mechanical systems. This paper differs from previous studies [10–12] since a strong nonlinearity is proposed here. This system (3) may exhibit types of motion unavailable in linear or weakly nonlinear vibration absorbers. The energy of vibrations is transferred to the second added oscillator and damped out in quasiperiodic regime and thus the attenuation of vibrations of the primary mass is achieved. Indeed, we will see that in the regime of quasiperiodic response the nonlinear oscillator ensures better suppression of oscillations than the best linear absorber with the same mass. In particular, this absorber seems to be quite effective during transient time [8,13]. That is why the use of this nonlinear absorber during real transient excitations (like real earthquake records) can be considered. The theoretical jump from sinusoidal forcing to earthquake is not obvious. However, the earthquakes considered in this study are seen as impulsions (a lot of energy in a very small time) and it appears from the response spectrum that those earthquakes have only one main peak so they are almost monochromatic. For example, consider accelerogram data from the Friuli (Italy, 06/05/1976) earthquake at the Tolmezzo-Diga Ambiesta station, the N-S horizontal component (all the earthquake data are extracted from the CD-rom "Strong Motion Database Navigator" (Copyright (c) 1996-2000 CubicSoft)). The response spectrum (i.e. the acceleration response spectrum) is displayed in Fig. 12. Let the parameters of Eq. (3) for the nonlinear attachment be: $\omega_2^2 = 8 \times 10^5$, $\varepsilon = 0.06$, $\lambda_2 = 8.17$ (so the specific natural damping in the nonlinear system is 0.46%). Energy pumping and attenuation of the linear oscillator occur as shown in Fig. 13. It appears that the vibrations of the added structure, after resonating, are totally destroyed at $t = 7.5$ s as shown in Fig. 13c. This phenomenon can be better seen in Fig. 14 where the intensity of the earthquake has been amplified. This figure shows that when the vibrations of the primary structure x_1 overcome a certain value (at $t = 4.7$ s), then the nonlinear added structure (x_2) resonates. Therefore, attenuation of x_1 occurs and we can clearly see the total destruction of x_2 at $t = 6$ s (brutal change of frequency) which guarantees a better attenuation (as we will see further) of vibrations of x_1.

It should be noted, in this example, that the maximum displacement is not necessarily attenuated significantly, since energy pumping occurs above a certain threshold value of amplitude. However, above this

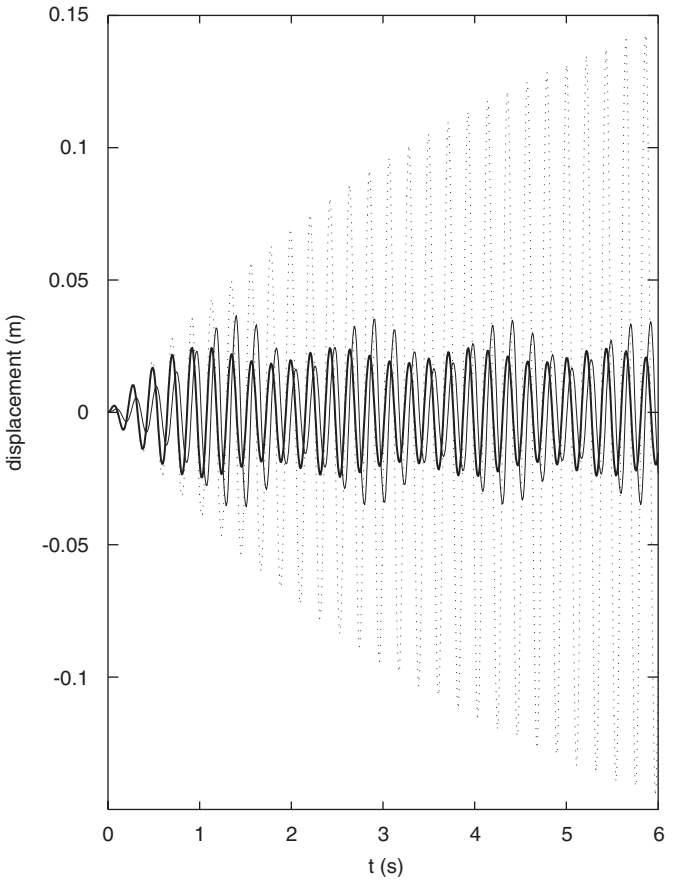

Fig. 10. Energy pumping with quasiperiodic vibrational regime. The dotted line - - - denotes the displacement of x_1 without coupling (i.e. the case in which no absorber is present), the thick line —— denotes the displacement of x_1 with coupling (i.e. the case in which the absorber is present) and the thin line — the displacement of x_2 with coupling.

threshold value, the vibrations are then attenuated efficiently. The magnitude of the power supplied, by the ground acceleration, to system (3) and particularly the timing of this supplied power is critical. In order to determine the efficiency of energy pumping it is necessary to use some indicator of supplied input power. Arias intensity is a measure of the total power supplied by the ground motion to the system. It correlates well with several commonly used demand measures of structural performances, liquefaction, and seismic slope stability. Arias intensity is defined by Arias [14] as

$$I_a = \frac{\pi}{2g}\int_0^\infty a(t)^2\,\mathrm{d}t, \tag{5}$$

where I_a is the Arias Intensity in units of length per time, g is the acceleration of gravity and $a(t)$ is the acceleration–time history in units of g. We can also define a modified Arias Intensity I_r of the responses of structures by

$$I_r = \frac{\pi}{2g}\int_0^\infty \ddot{x}_i(t)^2\,\mathrm{d}t, \quad i = 1, 2, \tag{6}$$

where $\ddot{x}_i(t)$, $i = 1, 2$ are the accelerations of the two structures in units of g. Thus, it is possible to plot the I_r of the response (acceleration) of structure as a function of the I_a of the earthquake excitation $\ddot{x}_g$. The Arias intensity of the ground motion typically increases with an increase in earthquake magnitude; though at larger

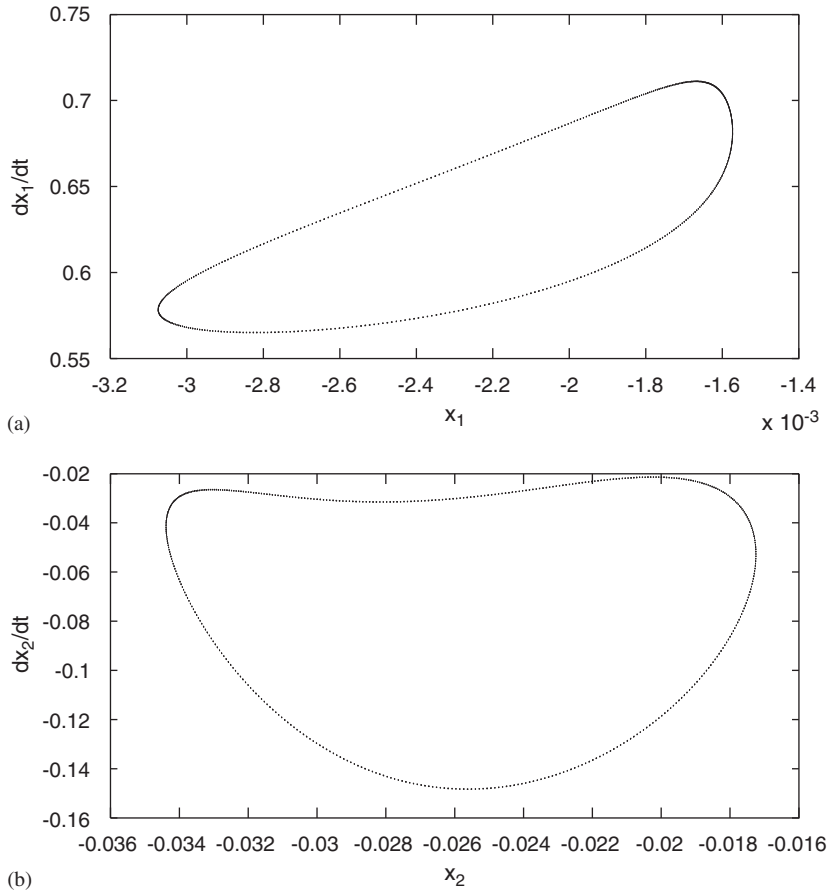

Fig. 11. Poincaré sections showing quasiperiodic vibrational regime (both figures are for the primary structure with nonlinear attachment: (a) for the primary structure; and (b) for the nonlinear attachment).

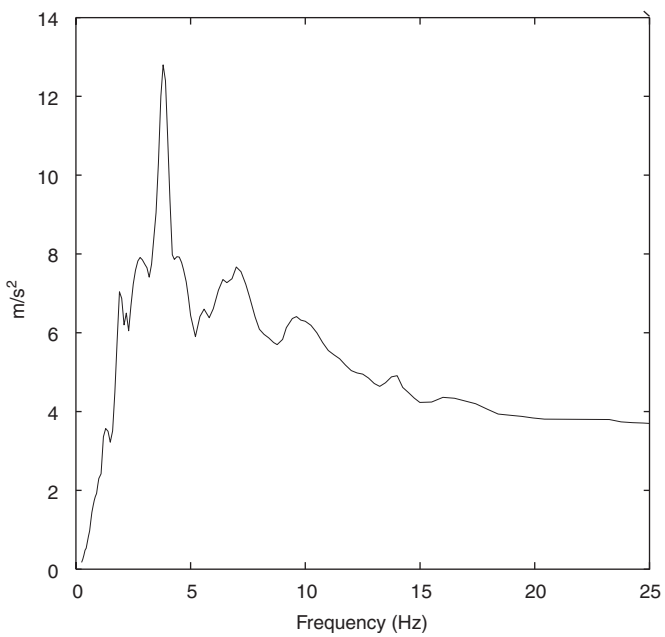

Fig. 12. Spectrum (i.e. the acceleration response spectrum) of a real earthquake in Friuli (Italy).

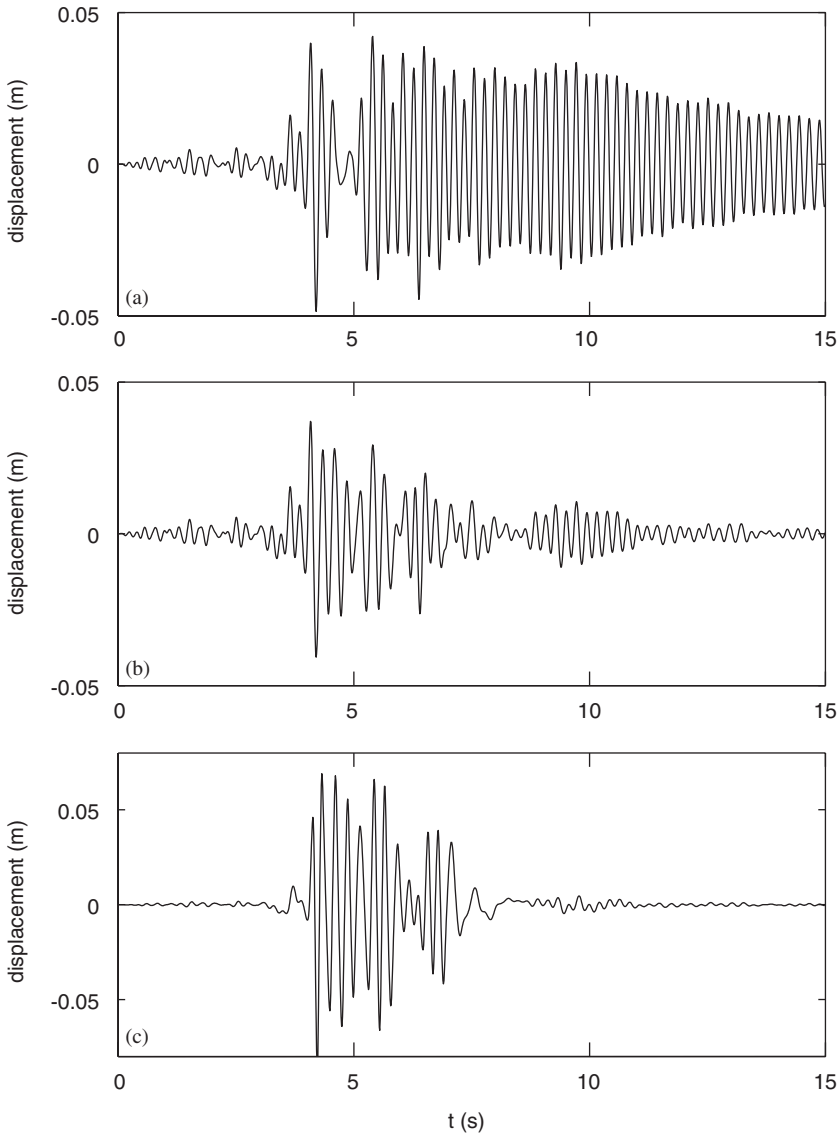

Fig. 13. Energy pumping with a real earthquake in Friuli (Italy); (a) primary structure without coupling (i.e. the case in which no absorber is present); (b) primary structure with coupling (i.e. the case in which the absorber is present); (c) attached structure with coupling.

earthquake magnitudes the relationship is not linear. Fig. 15 displays the excitation and response Arias intensities for the primary structural mass, the secondary mass and for the primary structure in the case in which no absorber is present. A log scale is used for axes in order to underline the nonlinear effects and the interest of energy pumping. Indeed, when no coupling is considered (the case in which no absorber is present), the plot is a line for a linear oscillator.

In this Fig. 15, the transfer of energy from the primary structure to the secondary one appears for the I_a of $\ddot{x}_g$ equals to $0.04\,\mathrm{m\,s^{-1}}$. Far from this point, curves are lines because the second oscillator behaves like a linear tuned mass damper. Energy pumping only occurs above this threshold value of amplitude. The attenuation of the acceleration of the primary mass occurs with the growth in acceleration of the secondary mass. The destruction of the resonance regime in the second structure results in an abrupt decrease of power of the primary mass. Consider Fig. 16 where two different amplitudes of ground motion have been applied; one below and one above the threshold value.

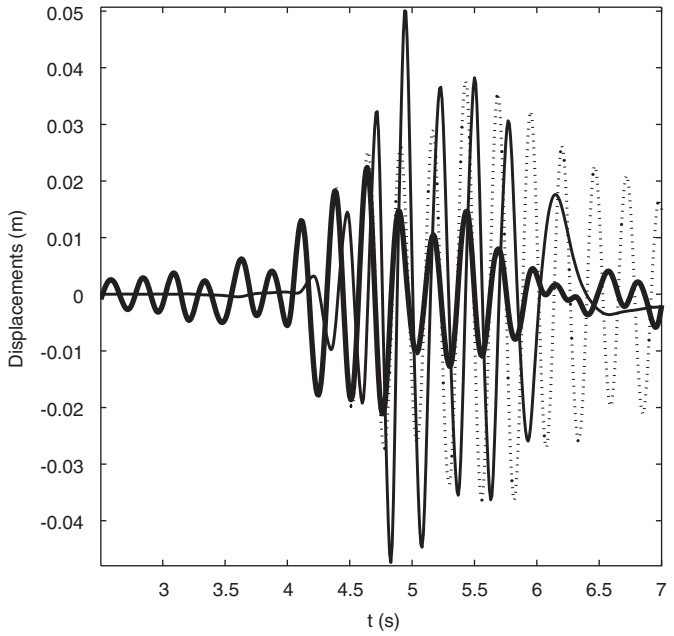

Fig. 14. Responses of the two structures: energy pumping with a real earthquake in Friuli (Italy). The thick line —— denotes x_1 with coupling, the solid line denotes x_2 with coupling and the dotted line - - - denotes x_1 without coupling.

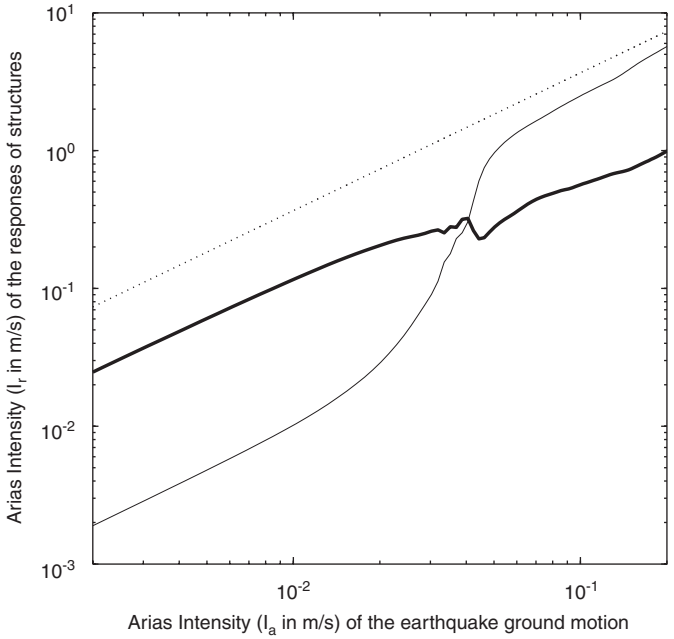

Fig. 15. Arias Intensity I_a with and without coupling. The primary structure without coupling is denoted by a dotted line - -, the primary structure with coupling is denoted by a thick line —— and the attached structure with coupling is denoted by a thin line —.

Moreover, for a periodic excitation and to better understand the interest of energy pumping compared to classical linear tuned mass damper, the amplitude–frequency curves can be plotted. For example, two cases can be compared: (i) a primary structure with an optimal linear tuned mass damper (the optimization is

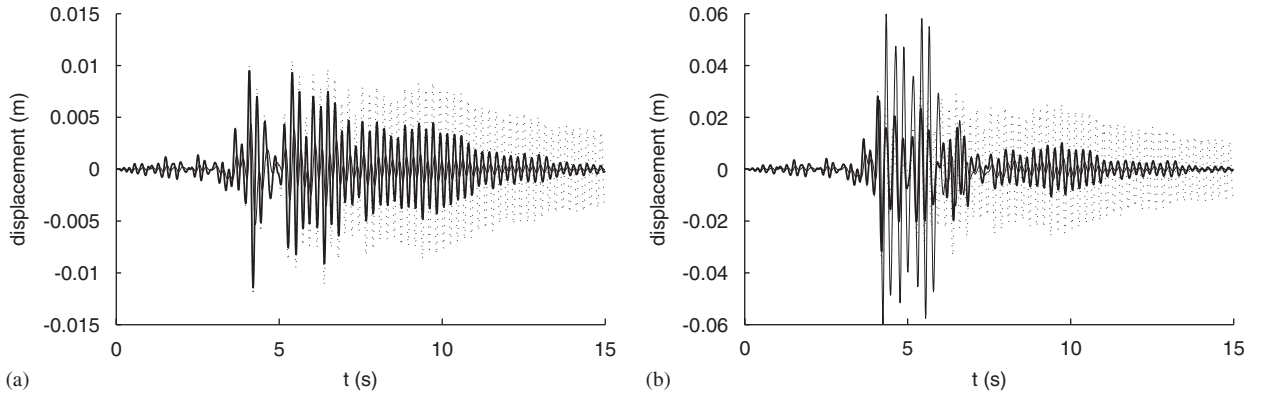

Fig. 16. Two different amplitudes of $\ddot{x}_g$ are considered; (a) amplitude $= 1\,\mathrm{m\,s^{-2}}$; (b) amplitude $= 3\,\mathrm{m\,s^{-2}}$, In (a) and (b), the dotted lines - - denote the displacements of x_1 without coupling, the thick lines —— denote the displacements of x_1 with coupling and the thin lines – the displacements of x_2 with coupling.

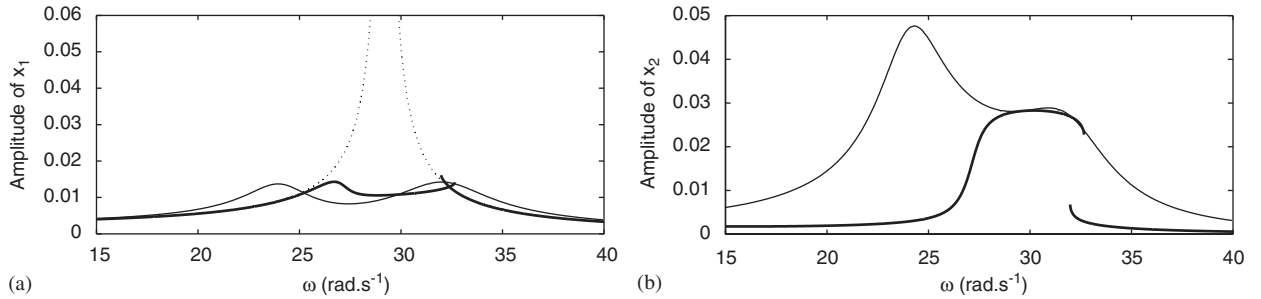

Fig. 17. Comparison with a tuned mass damper (TMD) by calculating the stable stationary regimes: (a) amplitude of $x_1(t)$; (b) amplitude of $x_2(t)$. The thick line —— denotes the amplitudes with the nonlinear coupling and the thin line — denotes the amplitudes with the linear TMD, the dotted line - - denotes the amplitude of x_1 without coupling.

described in Ref. [15]: $k_2 = 232.54\,\mathrm{N\,m^{-1}}$) (ii) a primary structure with a nonlinear attachment $\omega_2^2 = 8 \times 10^5$, $\varepsilon = 0.1$, $\lambda_2 = 7$ (so the specific natural damping in the nonlinear system is 0.39%). The damping coefficient and mass of the secondary added system are identical in both cases. Results are displayed in Fig. 17 for an harmonic excitation. The solutions for the nonlinear system have been calculated using the method described in Ref. [16]. The advantage of strong cubic coupling is that the curve with coupling (i.e. the case in which the absorber is present) is always under the curve without coupling (i.e. the case in which no absorber is present) and the main features of the primary structure to be isolated are not modified contrary to the addition of a classical Frahm damper. Indeed, in Fig. 17 for $20 < \omega < 25$, the linear absorber is not effective and it is even dangerous for the primary structure. As shown in Fig. 18 with a classical tuned mass damper and far from the main resonance two others peaks can appear. This latter point can be dangerous for the primary structure for example during an earthquake where several frequencies can be excited. The experiments confirm this point. The advantages and disadvantages of the two kinds of absorbers can be summarized in Table 1 in which the disadvantages have been underlined:

In the following theoretical analysis, the case of periodic excitation and the case of impulse with free oscillations ($G = 0$ but nonnull initial conditions) are both considered. All this theoretical study is mainly based on Ref. [17]. Change of variables:

$$v = x_1 + \varepsilon x_2, \quad w = x_1 - x_2 \tag{7}$$

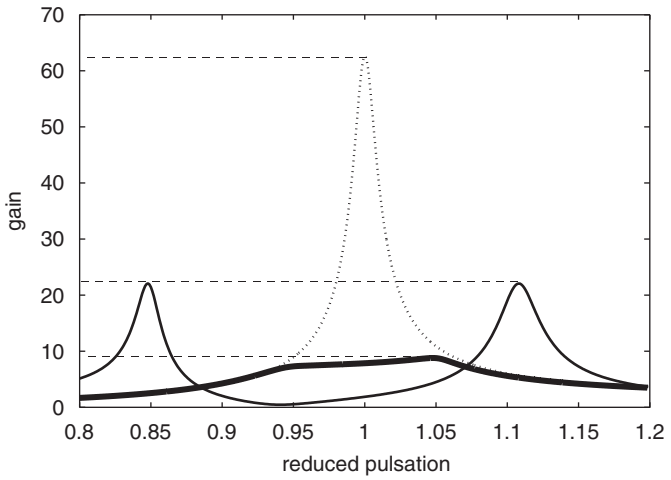

Fig. 18. Comparison with a classical tuned mass damper. The thick line —— denotes the cubic coupling, the solid line denotes the tuned mass damper and the dotted line - - denotes the curve without coupling.

Table 1
Comparison of the strongly nonlinear coupling with a linear tuned mass damper

Strongly nonlinear coupling	Linear tuned mass damper
Fitted to attenuate the whole frequency span of a mode	Fitted to attenuate a single frequency or narrow surrounding band
Reliable attenuation of natural frequency	Optimal attenuation of targeted frequency
Attenuation curve always remains underneath uncontrolled FrF	Possible amplification outside targeted frequency band-width
Little sensitive to frequency shifts FrF (structural damages, durability)	Sensitive to frequency shifts
Range of application:	Range of application:
Attenuation triggered beyond an amplitude threshold	attenuation as soon as low forcing amplitude levels
amplitude-dependent attenuation	attenuation gain independent from excitation level
Free oscillations: Yes/Steady vib.: Yes	Free oscillations: Yes/Steady vib.: Yes
Transient vibrations: Yes	Transient vibrations: No
Simultaneously control of several modes: cascades of resonances	No

allows reducing Eqs. (3) to the following form (where $G = \varepsilon F$):

$$\begin{cases} \ddot{v} + \dfrac{\varepsilon\lambda_1}{1+\varepsilon}\dot{v} + \dfrac{\varepsilon^2\lambda_1}{1+\varepsilon}\dot{w} + \dfrac{\omega_1^2}{1+\varepsilon}v + \dfrac{\omega_1^2\varepsilon}{1+\varepsilon}w = \varepsilon\omega_1^2 F\cos(\omega t) - \varepsilon^2\lambda_1 F\sin(\omega t), \\ \ddot{w} + \dfrac{\varepsilon\lambda_1}{1+\varepsilon}\dot{v} + \left(\dfrac{\varepsilon^2\lambda_1}{1+\varepsilon} + (1+\varepsilon)\lambda_2\right)\dot{w} + \dfrac{\omega_1^2}{1+\varepsilon}v + \dfrac{\varepsilon\omega_1^2}{1+\varepsilon}w + (\varepsilon+1)\omega_2^2 w^3 \\ \quad = \varepsilon\omega_1^2 F\cos(\omega t) - \varepsilon^2\lambda_1 F\sin(\omega t). \end{cases} \tag{8}$$

This change of variables physically corresponds to consideration of the center of masses and internal displacement of the system of oscillations. Then new small parameter is introduced and the dependent

variables are rescaled as follows:

$$\mathscr{X} = \varepsilon^{1/3}, \quad V = \mathscr{X}^{-1} v, \quad W = w. \tag{9}$$

With account of Eq. (9), System (8) is reduced to the following form (only terms up to order of $O(\mathscr{X}^2)$ are kept):

$$\begin{cases} \dfrac{\mathrm{d}^2 V}{\mathrm{d}t^2} + \omega_1^2 V + \mathscr{X}^2 \omega_1^2 W = \mathscr{X}^2 \omega_1^2 F \cos(\omega t), \\ \dfrac{\mathrm{d}^2 W}{\mathrm{d}t^2} + \lambda_2 \dfrac{\mathrm{d}W}{\mathrm{d}t} + \mathscr{X} \omega_1^2 V + \omega_2^2 W^3 = 0. \end{cases} \tag{10}$$

Now, a time-scaling is done by posing $\tau = \omega_1 t$, thus:

$$\begin{cases} \dfrac{\mathrm{d}^2 V}{\mathrm{d}\tau^2} + V + \mathscr{X}^2 W = \mathscr{X}^2 F \cos(\Omega \tau), \\ \dfrac{\mathrm{d}^2 W}{\mathrm{d}\tau^2} + a \dfrac{\mathrm{d}W}{\mathrm{d}\tau} + \mathscr{X} V + D W^3 = 0, \end{cases} \tag{11}$$

where $a = \lambda_2/\omega_1$, $D = \omega_2^2/\omega_1^2$ and $\Omega = \omega/\omega_1$. In the following studies, differentiation with respect to the variable τ (scaled-time) will be denoted by dots. As stated above, the goal of present investigation is the exploration of nonlinear normal modes of Eqs. (3) in the vicinity of 1:1 resonance (a 1:1 resonance is a resonance occurring between the two oscillators, each oscillating with the same frequency). It means that both variables, V and W, are supposed to have frequency close to unity (in the new time domain). Besides, the dynamics of the system is analyzed in the vicinity of the most dangerous resonance and therefore the frequency of the external excitation also is adopted to be close enough to unity:

$$\Omega = 1 + \mathscr{X}^3 \sigma. \tag{12}$$

Therefore, it may be adopted that both variables are expressed as

$$\begin{cases} V = \cos(\tau + \mu_1(\mathscr{X}\tau)) f_1(\mathscr{X}\tau), \\ W = \cos(\tau + \mu_2(\mathscr{X}\tau)) f_2(\mathscr{X}\tau), \end{cases} \tag{13}$$

where μ_i, $i = 1, 2$ takes into account phase shift and slow phase drift and f_i, $i = 1, 2$ slow amplitude modulation. We restrict ourselves by considering only phase trajectories with initial conditions inside the domain of attraction of 1:1 resonance manifold. Eqs. (11) may be reshaped to the following form:

$$\begin{cases} \ddot{V} + V + \mathscr{X}^2 W = \mathscr{X}^2 F \cos((1 + \mathscr{X}^3 \sigma)\tau), \\ \ddot{W} + W + \mathscr{X}(\delta[a\dot{W} + D W^3 - W] + V) = 0, \end{cases} \tag{14}$$

where $\delta = \mathscr{X}^{-1}$. If the estimation presented in Eqs. (13) is valid, then one obtains:

$$\ddot{W} = -\cos((1 + O(\mathscr{X}))\tau + \varphi_2) f_2(\mathscr{X}\tau) + O(\mathscr{X}) = -W + O(\mathscr{X}). \tag{15}$$

It means that in order to balance power 1 of small parameter $\mathscr{X}$ in the second equation of Eqs. (14), one must adopt

$$\delta[a\dot{W} + D W^3 - W] \sim O(1) \tag{16}$$

and therefore expression in square brackets should be of order $\mathscr{X}$. It is rather natural, as it describes slow modulation and damping of the vibrations with frequency close to unity. Then the theoretical study is similar to Refs. [17,18] so only final results are given in what follows. Indeed, after using complexification method [19] ($\psi_1 = \dot{V} + \mathrm{j}V$, $\psi_2 = \dot{W} + \mathrm{j}W$), by assuming fast oscillations ($\psi_i = \varphi_i \mathrm{e}^{\mathrm{j}\tau}$, $i = 1, 2$) and by introducing

multiple scale analysis [20]:

$$\varphi_k = \varphi_{k0} + \mathscr{X}\varphi_{k1} + \mathscr{X}^2\varphi_{k2}\ldots, \quad k = 1,2,$$

$$\tau_l = \mathscr{X}^l\tau, \quad \frac{\mathrm{d}}{\mathrm{d}\tau} = \frac{\partial}{\partial\tau_0} + \mathscr{X}\frac{\partial}{\partial\tau_1} + \mathscr{X}^2\frac{\partial}{\partial\tau_2} + \cdots \tag{17}$$

the following equation is obtained:

$$\frac{\partial\varphi_{20}}{\partial\tau_2} = \frac{F[\frac{6D}{8}\varphi_{20}^2\mathrm{e}^{-\mathrm{j}\sigma\tau_3} + (1+\mathrm{j}a - \frac{12D}{8}|\varphi_{20}|^2)\mathrm{e}^{\mathrm{j}\sigma\tau_3}] - \frac{18D}{8}\varphi_{20}|\varphi_{20}|^2 + (\mathrm{j}-a)\varphi_{20}}{2\delta(1+a^2 - \frac{24D}{8}|\varphi_{20}|^2 + \frac{108D^2}{64}|\varphi_{20}|^4)}. \tag{18}$$

For $0<a<\frac{1}{\sqrt{3}}$, Eq. (18) exhibits singularities due to possible nullification of the denominator. Indeed, for $0<a<\frac{1}{\sqrt{3}}$, a bifurcation occurs, i.e. "the regime of the nonlinear normal mode is broken down resulting in rather abrupt decrease of both amplitudes. The phase trajectory of the coupled system leaves the resonance manifold and the nonlinear normal mode is totally destroyed as a result of passage through the bifurcation" [17]. So, by considering an impulse for excitation with free oscillations, then under the critical value of a, the regime of the nonlinear normal mode is broken down with rather abrupt decrease of amplitudes x_1 and x_2, the second oscillator continues oscillating with the same frequency where as the first totally changes its behavior. This last point was underlined in Ref. [13]. In the case where the nonlinear damping is above the critical value, therefore no bifurcation of the invariant manifold exists so the damped nonlinear normal mode persists in all time domain. In Ref. [13], it was shown with energy studies that the passage of the phase trajectory through the bifurcation of the invariant manifold essentially facilitates the energy dissipation (more abrupt decrease of energy). So, by considering an impulse for excitation with free oscillations, this phenomenon will occur if:

$$0<a<\frac{1}{\sqrt{3}}, \text{ i.e. } c_2 < \frac{m_2\sqrt{k_1}}{\sqrt{3m_1}} \quad \text{or } \xi_{(\text{specific natural damping})} < \sqrt{\frac{4k_1m_2}{3k_2m_1}}. \tag{19}$$

Under constant external loading such branch structure may give rise to quasiperiodic oscillations (see, e.g. Ref. [21]). It means that in certain range of the external forcing intensity and the damping coefficient. System (3) is expected to demonstrate quasiperiodic oscillation regime instead of previously studied [16] periodic response. The numerical simulations of system (3) with zero initial conditions verify the later conclusion. Indeed, in Fig. 10, we have $a = 0.52 < \frac{1}{\sqrt{3}}$ and the plot demonstrates typical quasiperiodic behavior of both responses (x_1 and x_2). This behavior was also revealed for long-time simulations. In order to verify the suggested explanation of this phenomenon (breakdowns of motion on 1:1 resonance (i.e. resonance with the same frequency for each oscillator) invariant manifold due to singularities accompanied by successive attractions of the phase trajectory to another branch) we plot the internal coordinate of the system ($x_1 - x_2$) versus time (with the same parameters as previously in Fig. 10: $a = 0.5188$ and $D = 711$) and compare it with critical values of this function which correspond to singularities of Eq. (18) (Fig. 19). It is easy to see that the variation in peak amplitude of the internal coordinate follows the critical values with good accuracy and therefore the system primarily moves in different regimes resulting in quasiperiodic regime. The other argument in favor of the suggested scenario is that no quasiperiodic response was revealed for values of a above the range $0<a<\frac{1}{\sqrt{3}}$. The reason suggested is that for these values of the damping coefficient the bifurcation is no more possible. The Neimark bifurcation which occurs can be shown by a bifurcation diagram as shown in Fig. 20. This Fig. 20 shows the Poincaré's sections versus the parameter λ_2 with the same parameters as previously (for each section zero initial conditions are considered since in practical experimentation, the masses will be initially at rest). It should be noted that when $\lambda_2 > \lambda_{2\text{critical}}$ periodic solutions are found and when $\lambda_2 < \lambda_{2\text{critical}}$ quasiperiodic solutions are found. In this figure it can be clearly seen that under the critical value of damping ($\lambda_{2\text{critical}} = 15.8$), the oscillations of the nonlinear oscillator are stronger. If the amplitude of the external excitation is varying then the bifurcation can be seen as shown in

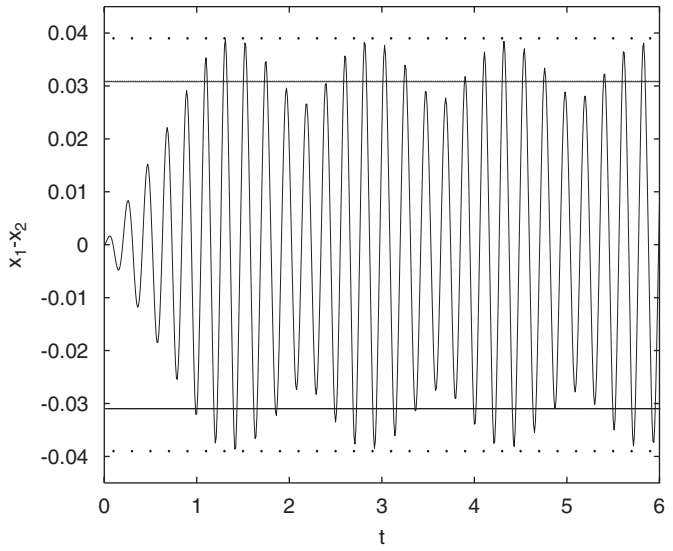

Fig. 19. Internal deformation $x_1 - x_2$ of the NES. Horizontal lines correspond to critical values of φ_{20} (linked to the internal deformation) computed from denominator of Eq. (18). Dotted line - - corresponds to upper boundary and solid line – to lower boundary.

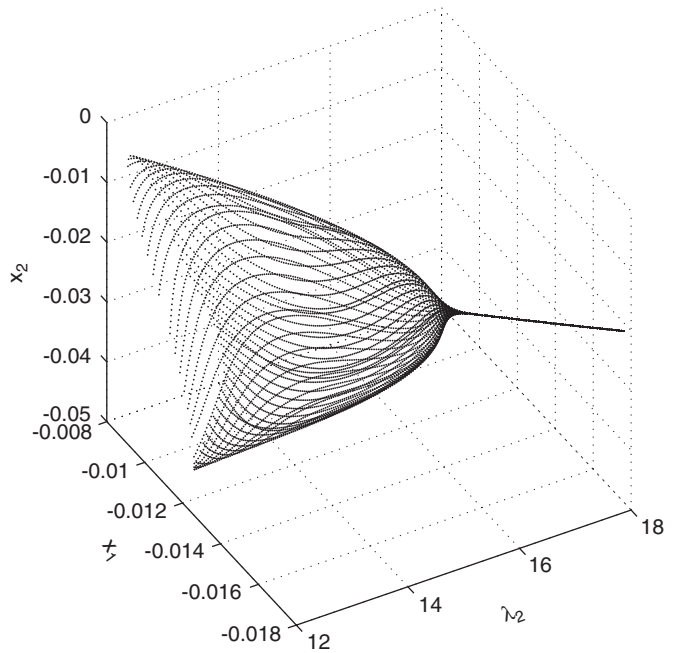

Fig. 20. Bifurcation diagram (versus the parameter λ_2).

Fig. 21. This Fig. 21 shows the Poincaré's sections versus the parameter $\omega_1^2 G$ with the same parameters as previously. It should be noted that quasiperiodic regime occurs only above a critical value of external excitation.

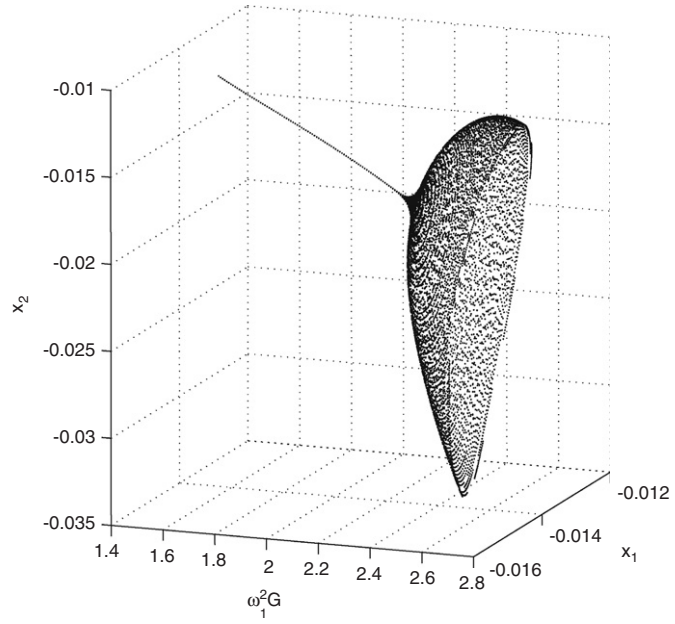

Fig. 21. Bifurcation diagram (versus the parameter $\omega_1^2 G$).

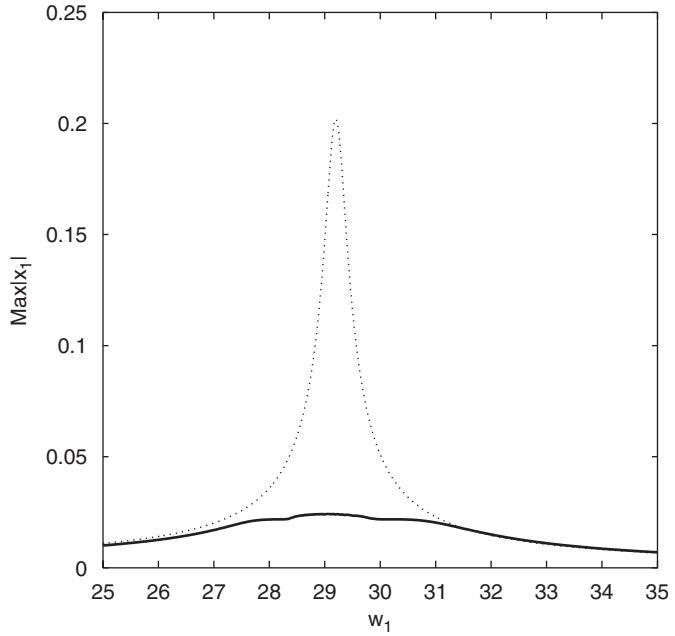

Fig. 22. Displacement response spectrum (the natural frequency ω_1 of the building is varying) with an external excitation $2.5\cos(29.2t)$. The solid line denotes the displacement of x_1 with coupling (i.e. the case in which the absorber is present) and the dotted line the displacement of x_1 with no coupling.

Moreover, the results can be generalized. The case we have considered is only for one set of (m_1, k_1), i.e. only one configuration of the building. It remains to explore the influence of natural frequency to underline the interest of such a nonlinear device compared to classical tuned mass damper. Thus, we can plot the

spectrum response, i.e. the displacement response spectrum: for different sets (m_1, k_1) (i.e. ω_1) of the building, we plot the peak (the maximum of the displacement) when a periodic forcing (of frequency $\omega = 29.2$ for each set (m_1, k_1)) is applied as illustrated in Fig. 22. Thus, this figure demonstrates some broadening of the suppression frequency range. This is a key advantage of the NES compared to classical tuned mass damper (The NES is more robust). Indeed, a classical tuned mass damper is adjusted and fitted for only one set of (m_1, k_1) but it is not efficient anymore if the stiffness is changing (because of the ageing of the structure for example).

As application, Fig. 13 shows the case of an earthquake excitation. In this figure, first we can clearly see the fact that when the primary structure overcomes a certain value (in Fig. 13b) at $t = 4$ s then the nonlinear structure resonates (in Fig. 13c). Secondly we can clearly see in Fig. 13c the fact that the nonlinear normal mode is totally destroyed at $t = 7.5$ s.

In the scope of this energy pumping validation, experimental measurements have to be investigated by mean of a suitable signal processing tool. Such a post-process must enable observation of expected resonance

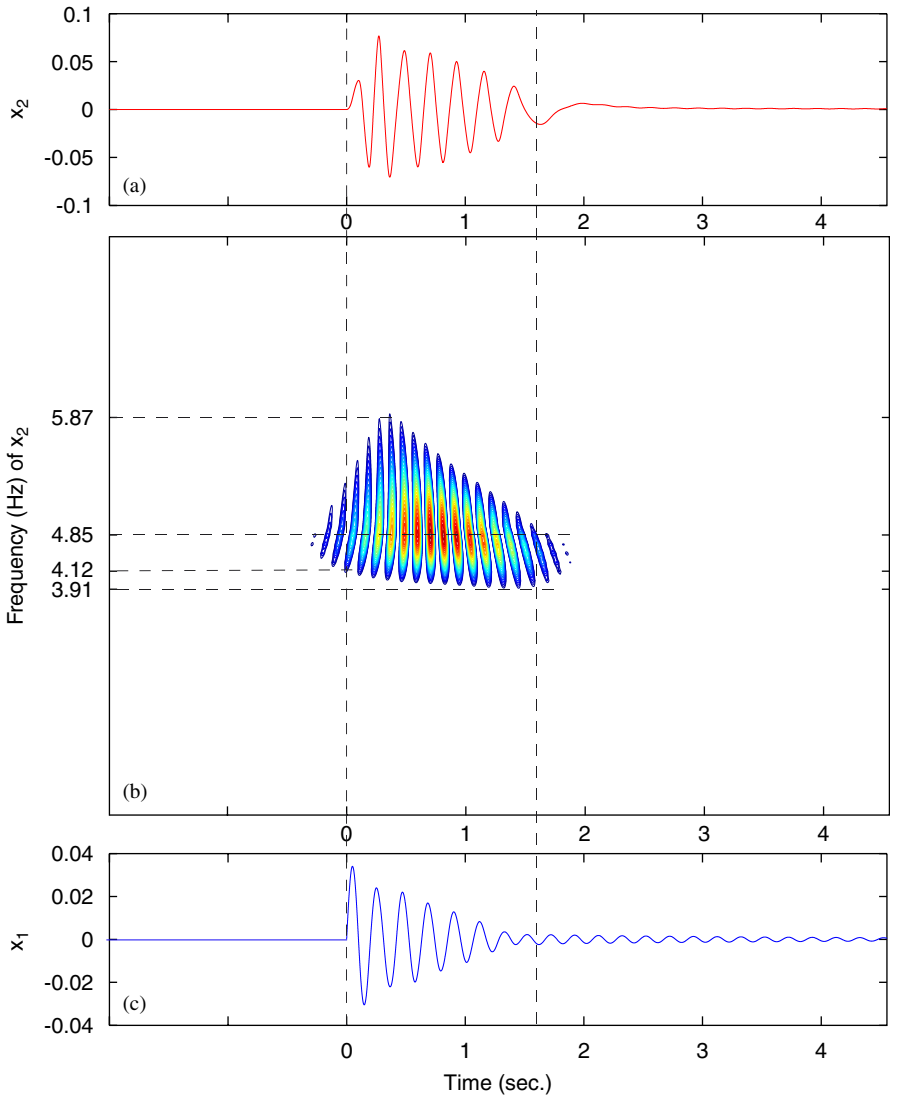

Fig. 23. Wavelet analysis with $\lambda_2 = 8$ ($h = 0.6$): (a) oscillations of x_2; (b) wavelet analysis of x_2; (c) oscillations of x_1.

captures and vanishing nonlinear normal modes with de-noising capabilities. The final aim is to accurately obtain instantaneous frequencies values. A new wavelet-based methodology, namely quasicontinuous mapping [22], is then applied to experimental measurements. This time-frequency analysis allows to thoroughly investigating experimental measurements. For instance frequencies superposition can be identified. It would appear in maps as a vertical juxtaposition of contours. Such an identification is very difficult with analysis such as Hilbert Transform [23] or dyadic wavelet analysis [24,25]. Moreover, a succession of contours with small radius during a temporal range $\delta\tau$ and within a constant frequency level ξ reveals the presence of a pattern with central frequency ξ on the time-interval $\delta\tau$. In addition a set of contours with small radius successively defined from frequency ξ_1 to frequency ξ_2 highlights a frequency migration on the frequency range $[\xi_1, \xi_2]$. A matlab interface program based on C++ wavelet library has been developed at "Laboratoire Géomatériaux" of "Ecole Nationale des Travaux Publics de l'Etat" that allows to quickly and accurately map experimental signals in the time–frequency half-plane. From this way the relevant frequency content of experimental measurements is investigated with inner de-noising capabilities of wavelet analysis. As concerned this study both resonant captures and nonlinear normal modes are highlighted and quantitatively investigated. For example, by taking $\varepsilon = 0.06$, $\lambda_2 = 8$ (so the specific natural damping in the nonlinear oscillator is 0.44%), $C = 8 \times 10^5$, $\omega_1 = 10\pi$, $F = 0$ (an impulse is considered) the critical value of nonlinear damping λ_2 is $10\pi/\sqrt{3}$. So by using the wavelet method, we can see in Fig. 23 (where the wavelet tools are used for x_2) that when $\lambda_2 = 8$ is under the critical value energy pumping is more efficient since the nonlinear normal mode is totally destroyed where as when $\lambda_2 = 22$ (so the specific natural damping of the

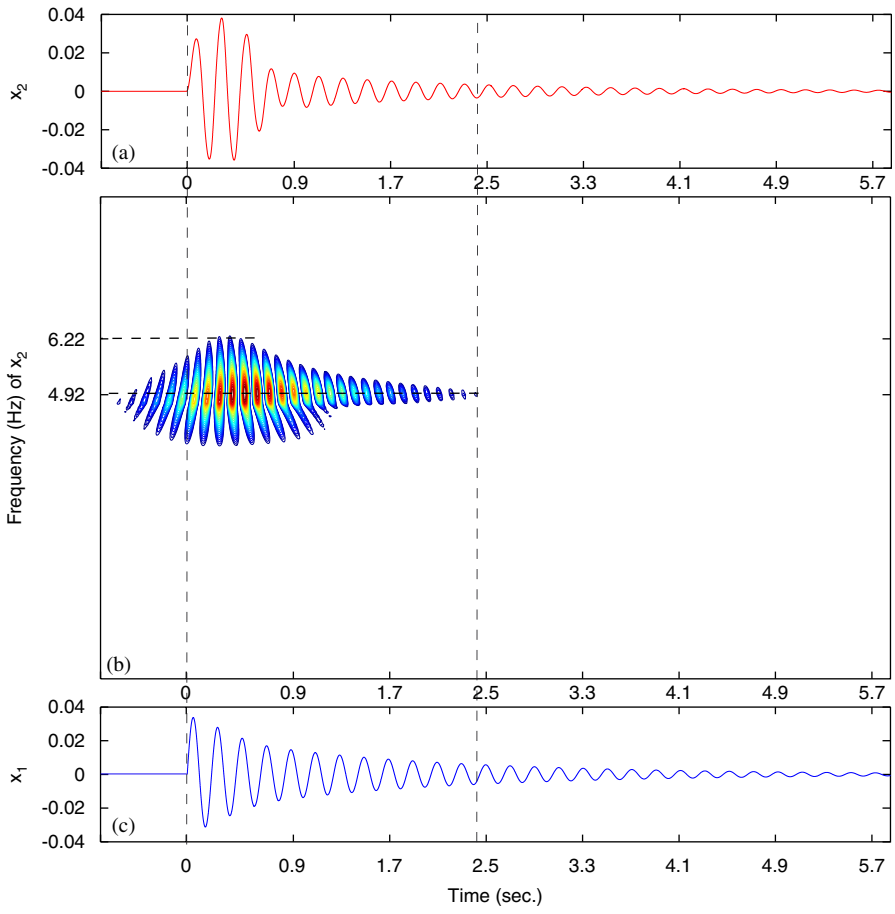

Fig. 24. Wavelet analysis with $\lambda_2 = 22$ ($h = 0.6$): (a) oscillations of x_2; (b) wavelet analysis of x_2; (c) oscillations of x_1.

nonlinear oscillator is 1.23%) is above the critical value energy pumping is less efficient since the nonlinear normal mode persists in all time domain as shown in Fig. 24.

Indeed, as shown in Fig. 23 thanks to the 1:1 resonance capture (around 5 Hz), energy is irreversibly transferred from the primary mass to the nonlinear attachment. It can also be observed that this nonlinear energy pumping is initiated by the excitation of transient modes as shown in Fig. 23b between 0 and 0.5 s (some higher frequencies are excited at the beginning of the response). Moreover, the nonlinear normal mode slightly decreases between 0 and 1.5 s (succession of contours with small radius but not at a constant level of frequency: the level of centers is decreasing around 4.85 Hz) and it is completely destroyed at $t = 1.5$ s which produces the quasi complete attenuation of the response of the primary structure as shown in Fig. 23c. In Fig. 24b, it clearly appears that the nonlinear normal persists in time domain between 0 and 2.5 s (succession of contours with small radius at a constant level of frequency 4.92 Hz) that is why no bifurcation occurs and the response of the primary structure is less attenuated as shown in Fig. 24c.

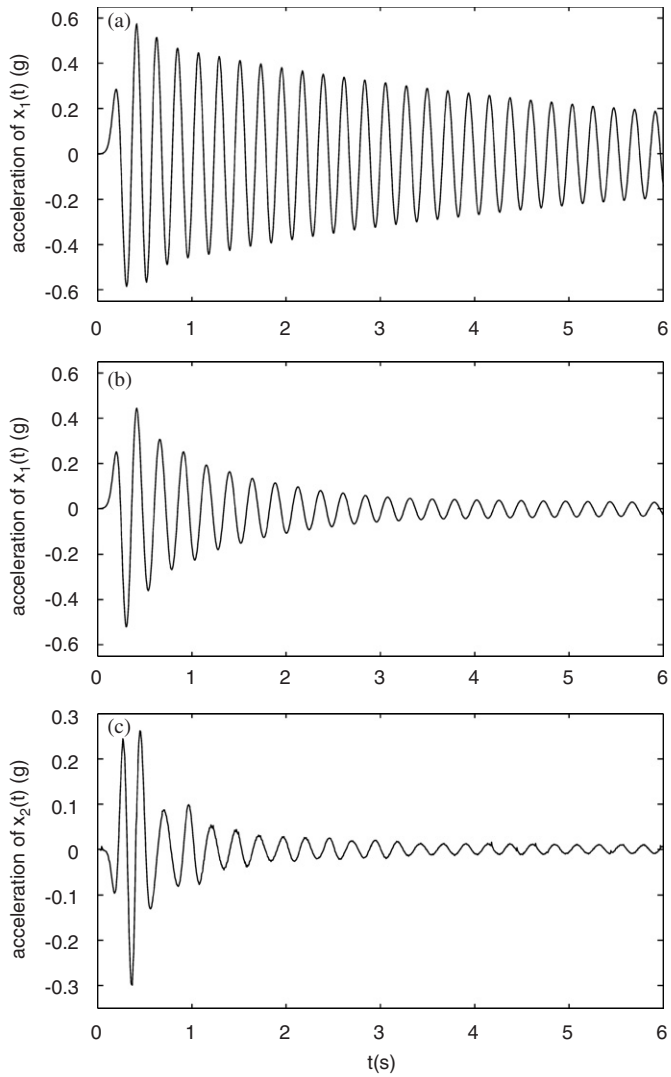

Fig. 25. Free oscillations with a nonnull initial displacement of the primary structure (impulsion at the upper plate): (a) free oscillations without coupling; (b) attenuation with coupling; (c) resonance of the secondary mass.

4. Experimental verification

First of all, to verify that when $0<a<\frac{1}{\sqrt{3}}$, the regime of the nonlinear normal mode is broken resulting in rather abrupt decrease of both amplitudes, the case of the absence of external forcing is considering. Indeed, first of all, impulse (on the upper part only) with free oscillations ($x_g = 0$) are considered. Experimentally, a nonnull initial displacement of the primary structure is considered with all other initial conditions null. This initial displacement is the same for studying the case with coupling (i.e. the case in which the absorber is present) and without coupling (i.e. the case in which no absorber is present). The different measured accelerations with and without coupling are given in Fig. 25.

Clearly, it appears that with the presence of the strongly nonlinear coupling, energy pumping occurs, i.e. attenuation of the acceleration of the primary structure with resonance of the nonlinear structure. Moreover, by using the wavelet analysis (for x_2) in Fig. 26, it is shown that the nonlinear normal mode (represented in

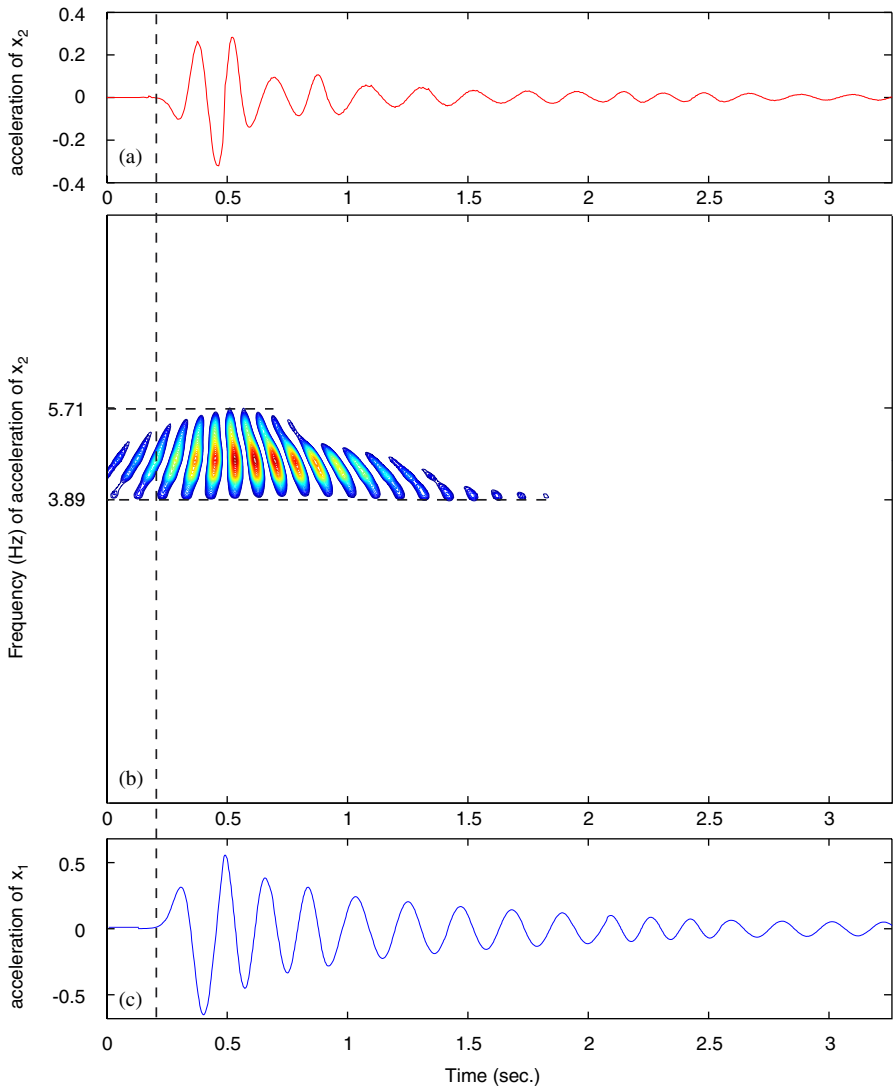

Fig. 26. Wavelet analysis of the experimental response with a nonnull initial displacement: (a) acceleration of x_2; (b) wavelet analysis of acceleration of x_2; (c) acceleration of x_1.

Fig. 26a) is totally destroyed through the passage of a bifurcation: the resonance occurs only between 0 and 1s and the nonlinear mode decreases as shown in Fig. 26b. It should be underlined that this phenomenon occurs only if the initial displacement of the primary structure is sufficient. This last point has been described in Ref. [2]. In this case, we have good agreement between experimental and numerical results.

Then, the case of periodic excitation with an external frequency closed to the natural frequency of the primary structure (i.e. 4.65 Hz) can be considered: an external forcing equals to 4.5 Hz is thus chosen (so $\sigma = -0.32$ with the notations of the previous section $\Omega = 1 + \varepsilon\sigma$). The experimental measured accelerations without the presence of the absorber and with presence of the strong coupling are plotted in Fig. 27 for

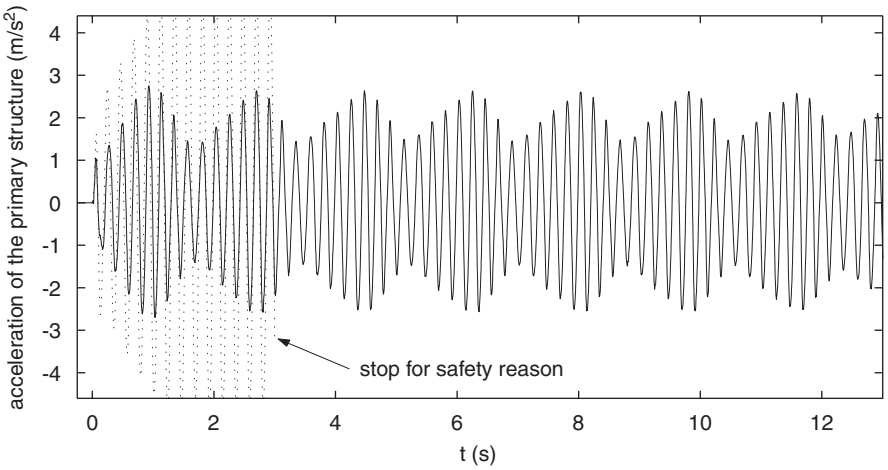

Fig. 27. Periodic transient forcing at a frequency closed to the internal frequency resonance. The dotted line - - denotes the vibrations without coupling and the thin line – denotes the vibrations with coupling.

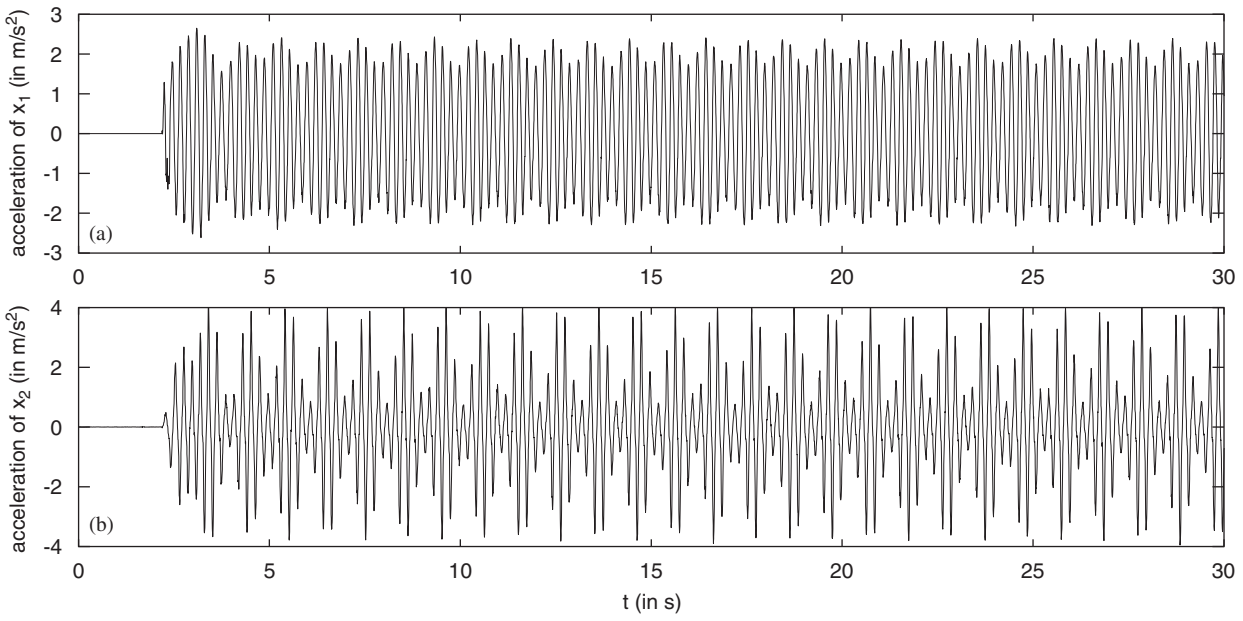

Fig. 28. Quasiperiodic responses of the two masses: (a) acceleration of x_1 (in m/s^2); (b) acceleration of x_2 (in m/s^2).

sufficient amplitude of the external forcing. It should be noted that for the case without coupling, we have stopped the external forcing at $t = 3$ s because the resonance became dangerous for the safety of the structure.

As shown in Fig. 27, absorption of vibrations in mechanical system is achieved with a good efficiency. Moreover, in the transient time, Fig. 27 shows that quasiperiodic phenomenon described in the theoretical study occurs. This motion appears to be clearly quasiperiodic motion and not transient behavior since it is still present after $t = 12$ s as shown in Fig. 28. In the transient time, by mean of wavelet analysis, Fig. 29 shows that jumps phenomena (i.e. brutal change of frequency due to bifurcation) described in the theoretical study occur. Moreover, as shown in Fig. 29b, during one phenomenon (for example between 1 and 2 s) we can clearly see that the nonlinear normal mode decreases (first 5.12 Hz, then 4.60 and 4.01 Hz): the nonlinear normal is destroyed; after there is the same resonance capture due to the continuous forcing. With Fig. 29c, it is underlined that when there is resonance of the nonlinear normal mode, the response of the primary structure is attenuated. Because of the continuous external forcing (with a frequency closed to the natural frequency of the linear structure), the linear response then increases again and energy pumping is activated only when the amplitude of the linear structure is above a certain value (for example at $t = 1$ or 3 s) as shown in Fig. 29c. This plot shows that, energy pumping occurs above a specific value of the initial energy level as underlined in

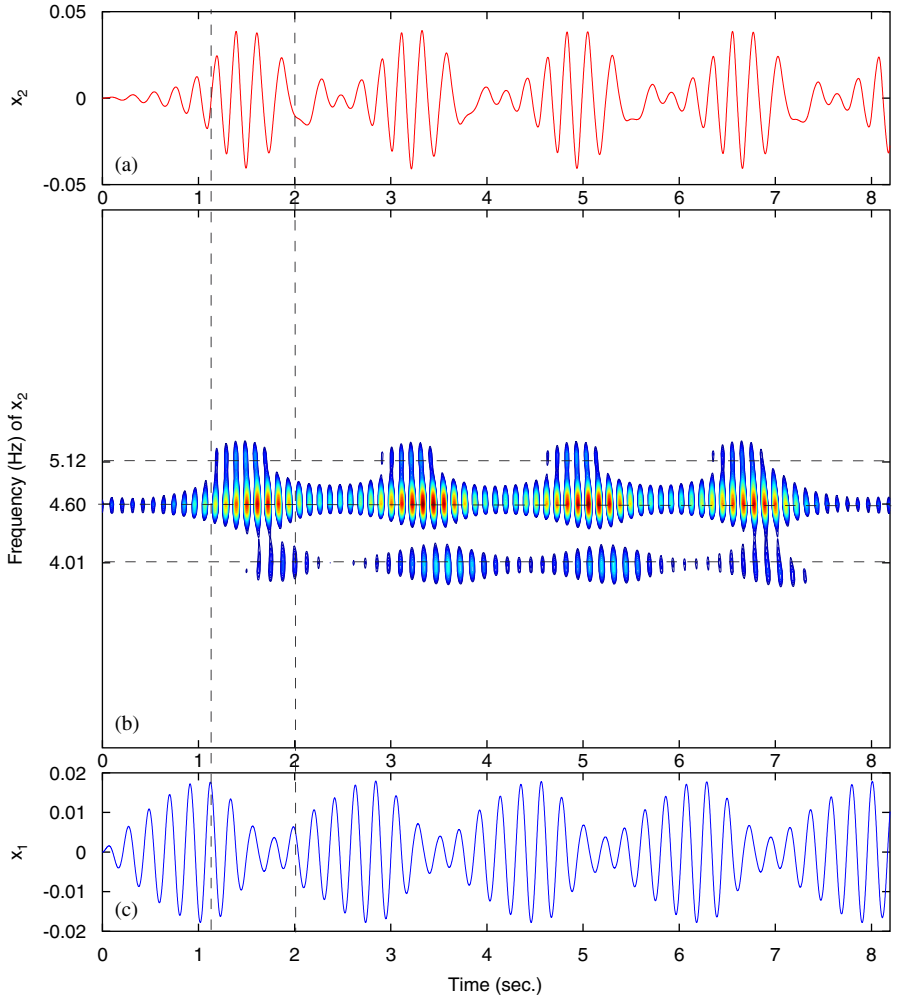

Fig. 29. Wavelet analysis of the quasiperiodic responses ($F = 0.03$): (a) oscillations of x_2; (b) wavelet analysis of x_2; (c) oscillations of x_1.

Ref. [26]: so when energy injected is too low, energy transfer from the linear structure to the nonlinear one does not appear. This quasiperiodic motion underlined in Ref. [17] is highlighted with the wavelet analysis. Thus, the presence of strong nonlinear coupling may exhibit types of motion (as seen in the previous part) unavailable for linear or weakly nonlinear vibration absorbers. However, the system under consideration exhibits this kind of response only for certain amplitude range of the external forcing otherwise it corresponds to periodic regime, which is less interesting than a linear tuned mass damper although some broadening of the suppression frequency range may be demonstrated. Indeed, when the amplitude of the external forcing is not

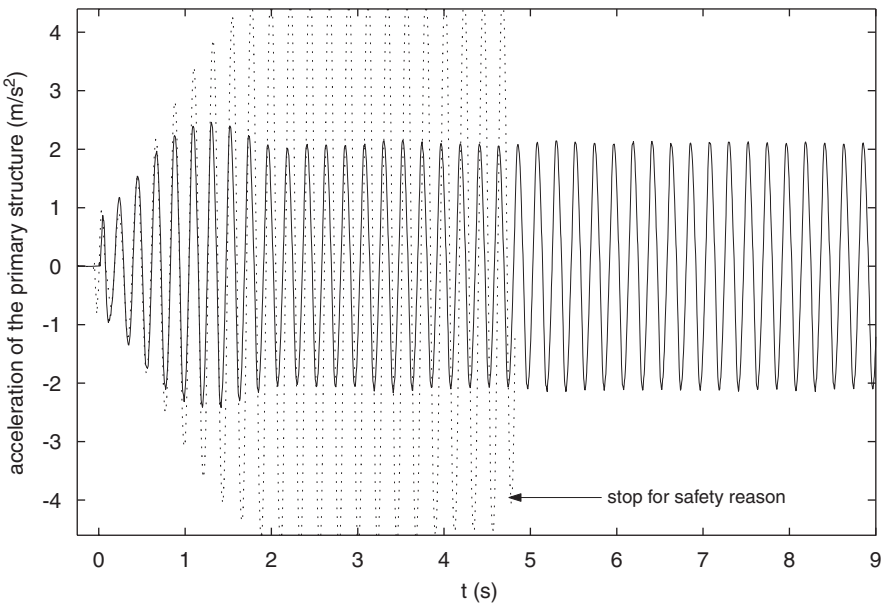

Fig. 30. Periodic transient forcing at a frequency closed to the internal frequency resonance without sufficient amplitude of forcing. The dotted line - - denotes the vibrations without coupling and the thin line – denotes the vibrations with coupling.

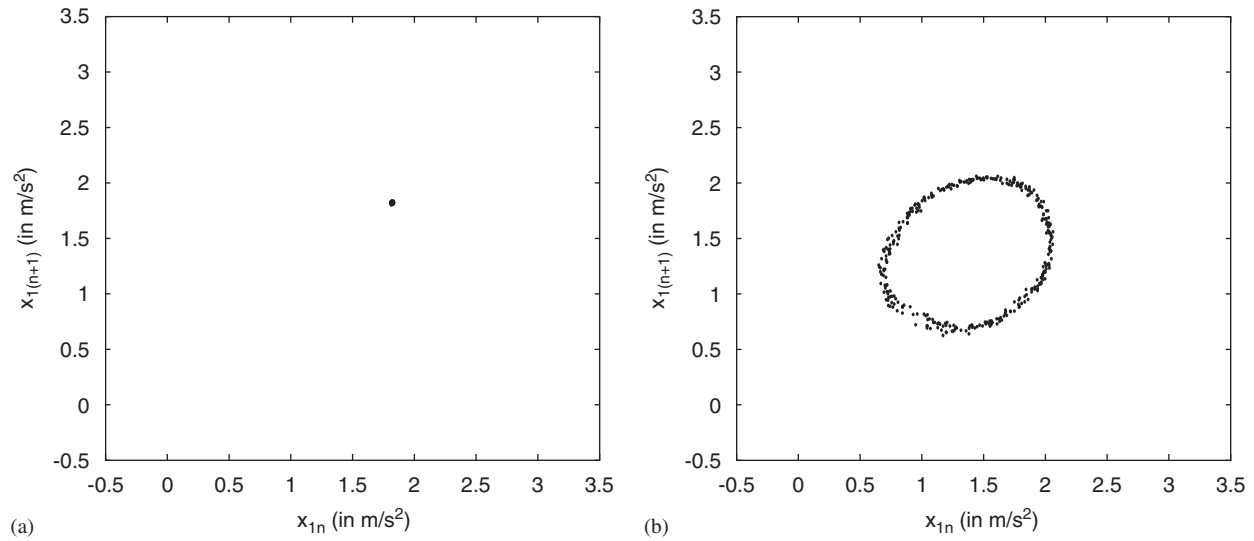

Fig. 31. Experimental first-return map: (a) periodic motion; (b) quasiperiodic motion.

enough sufficient, this quasiperiodic motion does not appear as shown in Fig. 30 (the Fig. 28 shows that the phenomenon of the quasiperiodic motion for x_1 and x_2 is a long time phenomenon).

To verify this quasiperiodicity (incommensurate frequencies), we can plot the experimental first-return map of the primary structure ($x_1(t)$) as shown in Fig. 31. This first return map is just derived from the *the Hénon trick* (explained in the third section) by plotting $x_{1(n+1)}$ versus x_{1n}. This first return map is often used for experimental (or numerical) data to avoid mixing results and uncertainties of several measured data issued from different accelerometers.

As shown in Fig. 31, the first-return map is either a point (so a periodic motion) as shown in Fig. 31a, either a closed loop (as shown in Fig. 31b), so a quasiperiodic motion when the forcing amplitude is above a certain value. The experimental results confirm the numerical ones.

Moreover, as underlined in the previous section, one possible application is related to absorption of vibrations particularly during earthquakes where the forcing occurs during the transient time. The actuator is piloted in displacement by a function generator (TTi 40 MHz Arbitrary Waveform Generator TGA 1241) in which it is possible to load a desired signal. All the earthquake data are extracted from the CD-rom "Strong Motion Database Navigator" (Copyright (c) 1996–2000 CubicSoft). Those data are transformed in terms of displacements to apply them to the small building model. For instance, we can apply to the primary structure

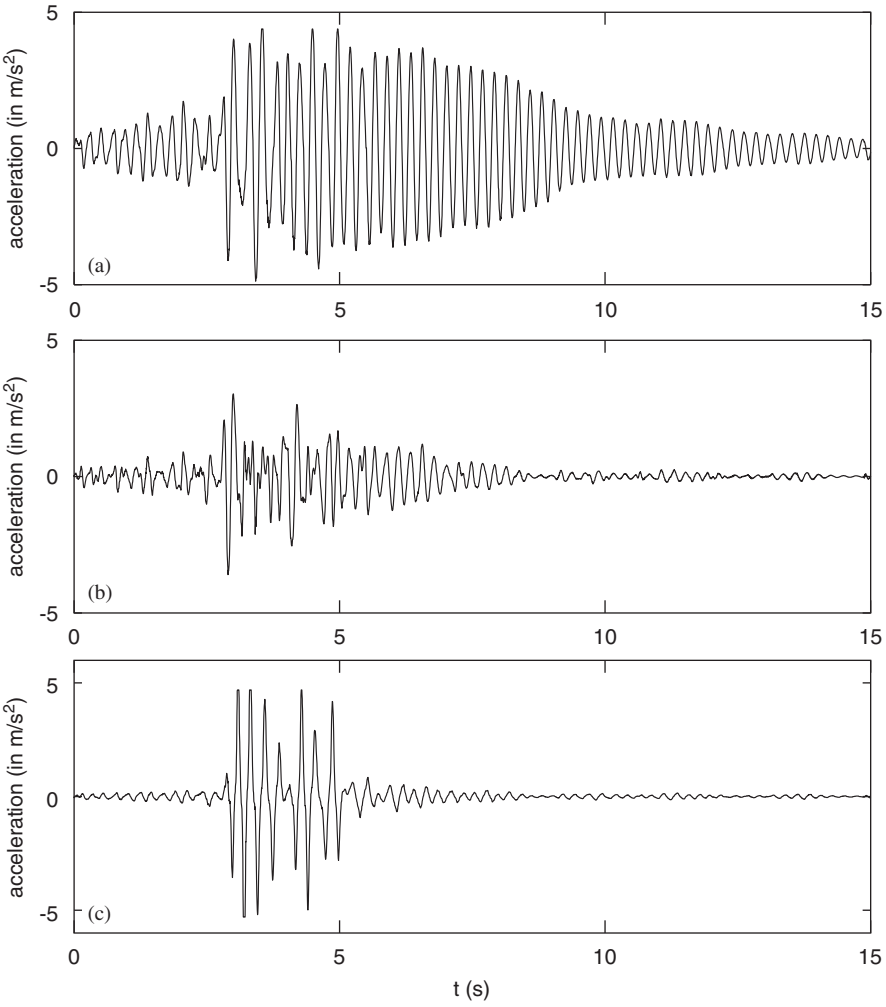

Fig. 32. Experimental results with a real earthquake forcing (Friuli in Italy): (a) primary structure (x_1) without coupling; (b) primary structure (x_1) with coupling; (c) attached structure (x_2) with coupling.

the earthquake of Friuli (Italy) (the same as the numerical studies; the peak acceleration of the accelerogram is scaled to equals $4\,\mathrm{m\,s^{-2}}$ and then is transformed into displacement) with the presence of the absorber and without the presence of the strong coupling (i.e. without absorber). The results are presented in Fig. 32.

In Fig. 32, the NES appears to be efficient as vibration absorber for transient forcing. In this figure, we can perfectly see the effect of NES: indeed, when the energy is transferred to the second mass (resonance of x_2) then the nonlinear normal mode is destroyed (abrupt decrease of x_2 for instance at $t = 5\,\mathrm{s}$ in Fig. 32c) which has for consequence to dissipate the vibrations of x_1 instantaneously. As described previously in the numerical study, the maximum of the response of the primary structure with coupling (Fig. 32b) may be still important but after this point, in time, the vibrations are attenuated with a good efficiency. That is why, it is possible to verify experimentally the curve of the Arias Intensity I_a by changing the intensity of the earthquake ground motion and to see the transfer of energy. Experimental results and numerical one are in good agreement as shown in Fig. 33.

Nevertheless, it should be underlined that the maximum peak can be attenuated a lot depending on the earthquakes. For example, if the Annecy earthquake (France, 15/07/1996) is considered, then the maximum peak is attenuated with a ratio of 60% as shown in Fig. 34.

Moreover, the results can be generalized. The case we have considered looks very convincing, however, it is only for one set of (m_1, k_1), i.e. only one configuration of the building. It remains to explore the influence of natural frequency to underline the interest of such a nonlinear device compared to classical tuned mass damper. Thus, we can plot the spectrum response, i.e. the displacement response spectrum: for different sets (m_1, k_1) (i.e. ω_1) of the building, we plot the peak (the maximum of the displacement) when the excitation is the Annecy earthquake as illustrated in Fig. 35. Thus, this figure demonstrates some broadening of the suppression frequency range. This is a key advantage of the NES compared to classical tuned mass damper (the NES is more robust). Indeed, a classical tuned mass damper is adjusted and fitted for only one set of (m_1, k_1) but it is not efficient anymore if the stiffness is changing (because of the ageing of the structure for example).

In order to show that this study is not only dependent on a specific earthquake, Fig. 36 displays similar results with Alkion earthquake (Greece, 24/02/1981, station of Xilokastro-OTE; the peak acceleration of the

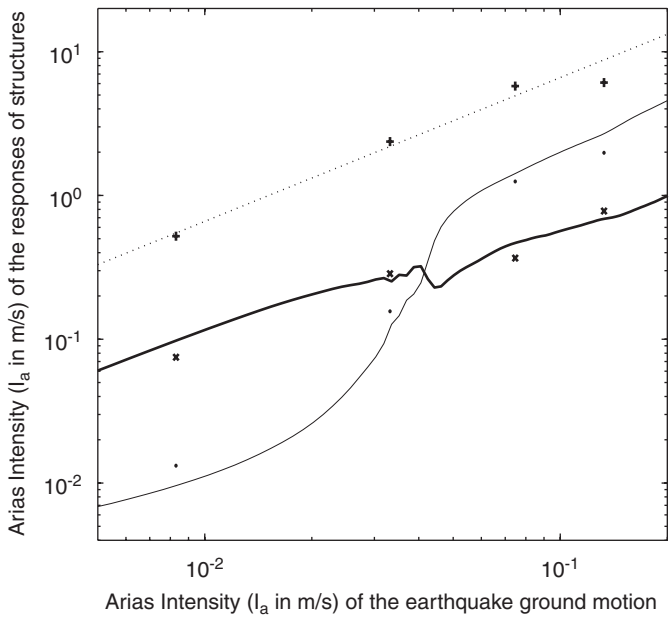

Fig. 33. Experimental results for the Arias Intensity I_a. The primary structure without coupling is denoted by a dotted line - -, the primary structure with coupling is denoted by a thick line —— and the attached structure with coupling is denoted by a thin line –. + denotes the experimental x_1 without coupling, · denotes x_2 with coupling, × denotes x_1 with coupling.

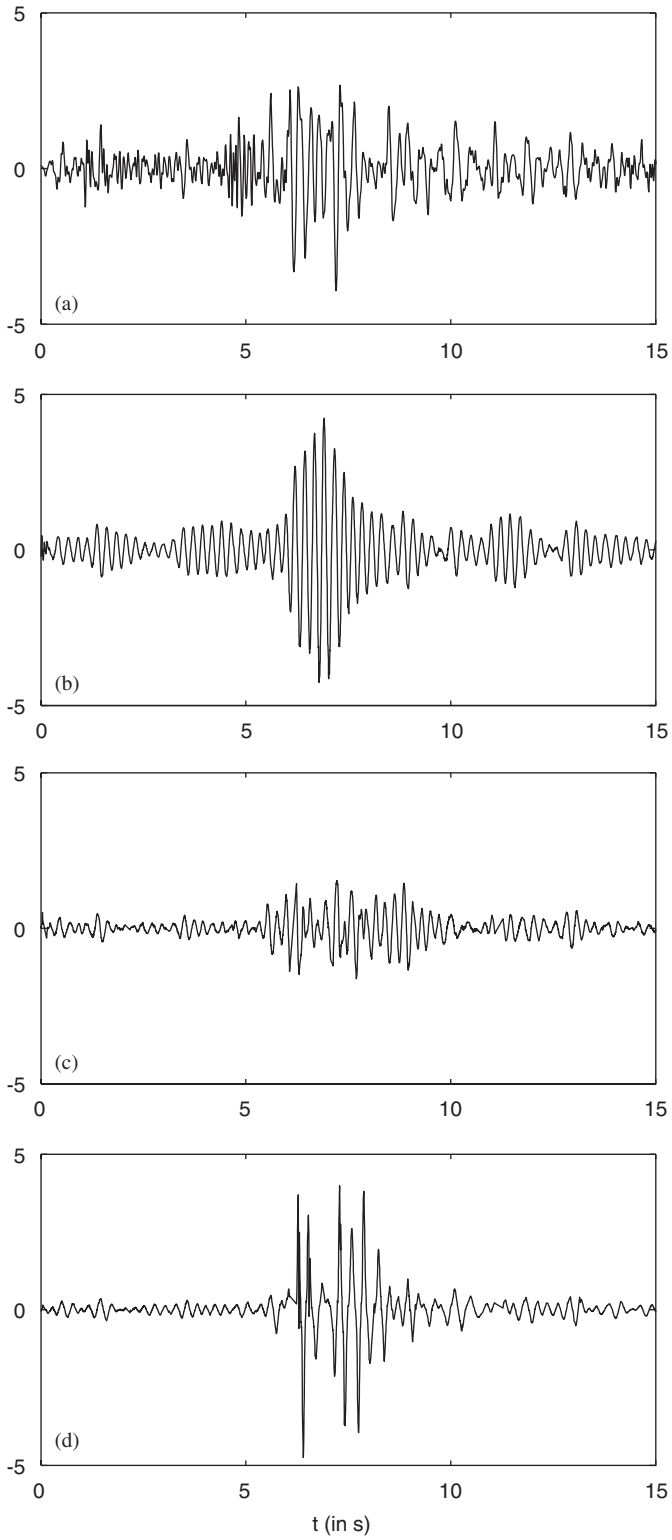

Fig. 34. Experimental results with a real earthquake forcing (Annecy in France): (a) acceleration of x_g (in $\mathrm{m\,s^{-2}}$); (b) acceleration of x_1 (in $\mathrm{m\,s^{-2}}$) without coupling; (c) acceleration of x_1 (in $\mathrm{m\,s^{-2}}$) with coupling; (d) acceleration of x_2 (in $\mathrm{m\,s^{-2}}$) with coupling.

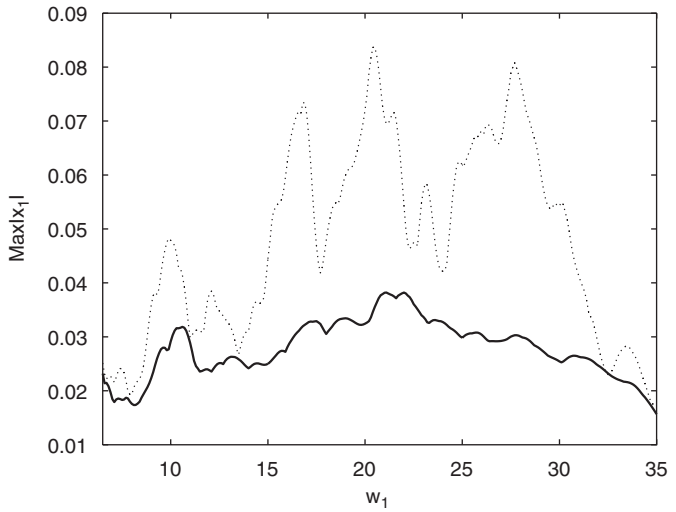

Fig. 35. Displacement response spectrum (the natural frequency ω_1 of the building is varying) with the Annecy earthquake. The solid line denotes the displacement of x_1 with coupling (i.e. the case in which the absorber is present) and the dotted line the displacement of x_1 with no coupling.

accelerogram is scaled to equals $2\,\mathrm{m\,s^{-2}}$ and then is transformed into displacement) which has been applied to the primary structure. In Figs. 32, 34, 36, there is resonance of the nonlinear added structure so attenuation of the vibrations of the primary structure.

5. Conclusion

Experimental verification of analytic and numerical results of nonlinear energy pumping has been performed by means of appropriately small designed building model. The experimental results demonstrate that the system exhibits the energy pumping from "large" to "small" mass by mechanism of 1:1 resonance, accompanied by generation of quasiperiodic vibrations. The quasiperiodicity has been found experimentally for the small building model. That is why, experimental results demonstrate that the quasiperiodic response regime associated with energy transfer to NES can be applied in Civil Engineering systems (the different parameters have been chosen to correspond to Civil Engineering problems). One possible application is related to absorption of vibrations in mechanical systems. Attenuation of the primary structure is achieved owing to this strong nonlinear coupling. In particular, the system appears to be quite effective with different earthquake excitations. For practical applications, it is very interesting since it is difficult to attenuate a lot of energy in a very short time owing to the classical tuned mass damper. Moreover, the added mass with the NES can be smaller than with classical tuned mass damper which is very interesting for practical applications. The case we have considered looks very convincing, and as underlined in the present study, it is not only for one set of (m_1, k_1), i.e. only one configuration of the building. Indeed, the influence of natural frequency has been explored. Some broadening of the suppression frequency range has been illustrated, so the results have been generalized. Indeed, in practical applications the natural frequency is changing (because of the ageing of the structure for example). In this case, the NES will be effective, which is not the case with classical tuned mass dampers which are fitted for one specific natural frequency (no additional design/adjustment is necessary with the NES). Then, the theoretical jump from sinusoidal forcing to earthquake is not obvious. However, the numerous experimental and numerical results show the good efficiency of such a NES for different earthquakes. Then, the system under consideration exhibits the desired behavior only for certain amplitude range of the external forcing and the phenomenon occurs only above a certain amplitude. The aim for further research is to achieve broader range of quasiperiodic response. In particular, the use of multiple nonlinear

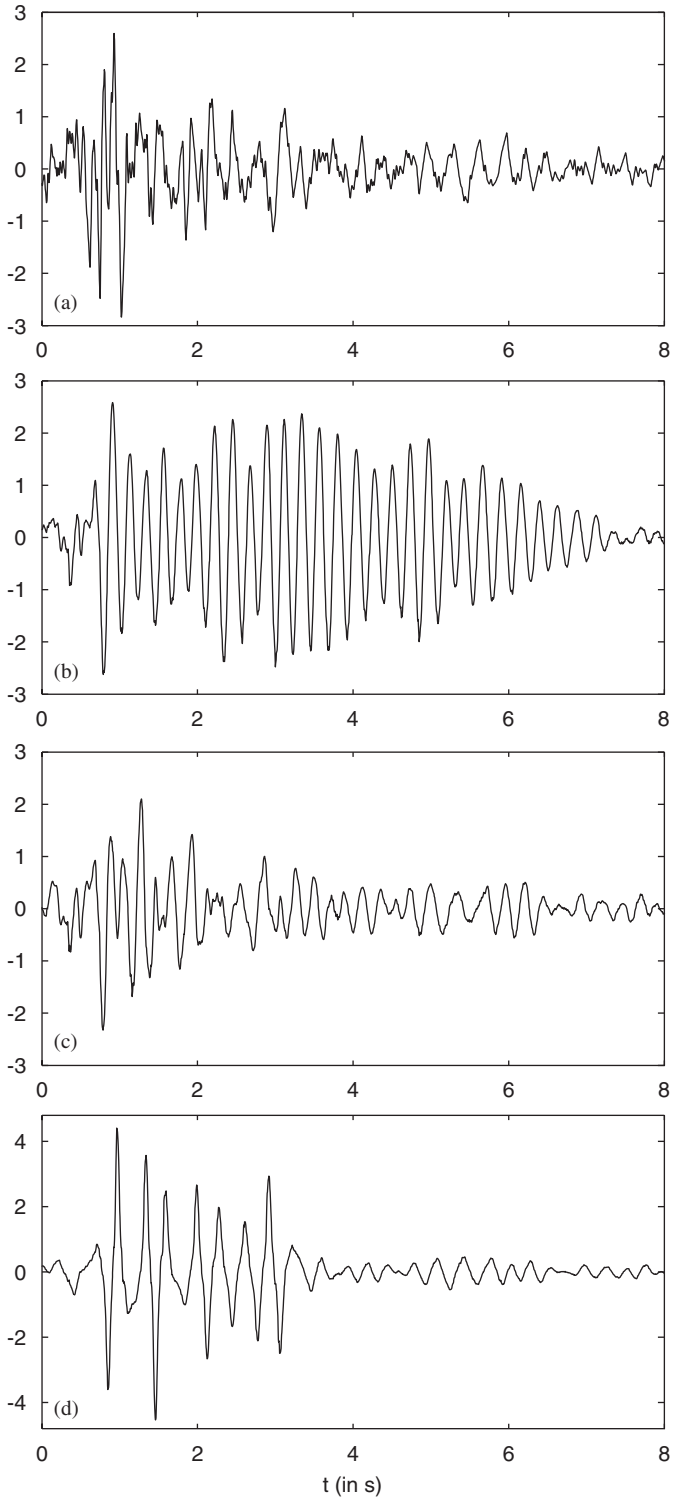

Fig. 36. Experimental results with a real earthquake forcing (Alkion in Greece): (a) acceleration of x_g (in $\mathrm{m\,s^{-2}}$); (b) acceleration of x_1 (in $\mathrm{m\,s^{-2}}$) without coupling; (c) acceleration of x_1 (in $\mathrm{m\,s^{-2}}$) with coupling; (d) acceleration of x_2 (in $\mathrm{m\,s^{-2}}$) with coupling.

normal modes (as described in Ref. [23]) can increase the span in amplitude of injected energy where the energy pumping phenomenon occurs.

Acknowledgements

This work was supported by Marie Curie Fellowship contract HPMT-CT-2000-00001 in part and was partially supported by Région Rhône-Alpes in the frame of Emergence Program "Pompage énergétique: théorie, faisabilité, expérience".

References

[1] A.F. Vakakis, A.N. Kounadis, I.G. Raftoyiannis, Use of nonlinear localization for isolating structures from earthquake-induced motions, *Earthquake Engineering and Structural Dynamics* 28 (1999) 21–36.
[2] A.F. Vakakis, L.I. Manevitch, O. Gendelman, L. Bergman, Dynamics of linear discrete systems connected to local, essentially nonlinear attachments, *Journal of Sound and Vibration* 264 (2003) 559–577.
[3] O.V. Gendelman, Transition of energy to a nonlinear localized mode in a highly asymmetric system of two oscillators, *Nonlinear Dynamics* 25 (2001) 237–253.
[4] O. Gendelman, L.I. Manevitch, A.F. Vakakis, R.M. Closkey, Energy pumping in nonlinear mechanical oscillators: Part I—dynamics of the underlying Hamiltonian systems, *Journal of Applied Mechanics* 68 (2001) 34–41.
[5] A.F. Vakakis, O. Gendelman, Energy pumping in nonlinear mechanical oscillators: Part II—resonance capture, *Journal of Applied Mechanics* 68 (2001) 42–48.
[6] O. Gendelman, L.I. Manevitch, A.F. Vakakis, L. Bergman, A degenerate bifurcation structure in the dynamics of coupled oscillators with essential stiffness nonlinearities, *Nonlinear Dynamics* (2003).
[7] E. Gourdon, C.H. Lamarque, Energy pumping with various nonlinear structures: numerical evidences, *Nonlinear Dynamics* 40 (2005) 281–307.
[8] D. McFarland, L. Bergman, A. Vakakis, Experimental study of non-linear energy pumping occurring at a single fast frequency, *International Journal of Non-Linear Mechanics* 40 (2005) 891–899.
[9] P. Hagedorn, *Non-linear Oscillations*, Clarendon Press, Oxford, 1988.
[10] G.S. Agnes, Performance of Nonlinear Mechanical, Resonant-Shunted Piezoelectric, and Electronic Vibration Absorbers for Multi-Degree-of-Freedom Structures, PhD Thesis, Virginia Polytechnic Institute and State University, 1997.
[11] F.R. Arnold, Steady-state behavior of systems provided with nonlinear dynamic vibration absorbers, *Journal of Applied Mechanics* 22 (1955) 487–492.
[12] J.B. Hunt, J.C. Nissen, The broadband dynamic vibration absorber, *Journal of Sound and Vibration* 83 (1982) 573–578.
[13] O.V. Gendelman, D.V. Gorlov, L.I. Manevitch, A.I. Moussienko, Dynamics of coupled linear and essentially nonlinear oscillators with substantially different masses, *Journal of Sound and Vibration* 286 (1–2) (2005) 1–19.
[14] A. Arias, A measure of earthquake intensity, *Seismic Design for Nuclear Power Plants*, MIT Press, Cambridge, MA, 1970, pp. 438–483.
[15] J.P. Den Hartog, *Mechanical Vibration*, McGraw-Hill, New York, 1947.
[16] X. Jang, D.M. McFarland, L.A. Bergman, A.F. Vakakis, Steady state passive nonlinear energy pumping in coupled oscillators: theoretical and experimental results, *Nonlinear Dynamics* 33 (2003) 87–102.
[17] O.V. Gendelman, E. Gourdon, C.H. Lamarque, Quasiperiodic energy pumping in coupled oscillators under periodic forcing, *Journal of Sound and Vibration*, 249 (2006) 651–662.
[18] O.V. Gendelman, Bifurcations of nonlinear normal modes of linear oscillator with strongly nonlinear damped attachment, *Nonlinear Dynamics* 37 (2) (2004) 115–128.
[19] L.I. Manevitch, Complex representation of dynamics of coupled nonlinear oscillators, *Mathematical Models of Nonlinear Excitations Transfer, Dynamics, and Control in Condensed Systems and Other Media*, Kluwer Academic Press, Plenum Publishers, New York, 1999, pp. 269–300.
[20] Ali.H. Nayfeh, *Perturbation Methods*, Wiley, New York, February 1973.
[21] E.A. Jackson, *Perspectives of Nonlinear Dynamics*, vol. 1, Cambridge University Press, Cambridge, 1994.
[22] S. Pernot, Méthodes Ondelettes pour l'étude des Vibrations et de la Stabilité des Systèmes Dynamiques, Thesis in Civil Engineering, Institut National des Sciences Appliquées, Lyon, France, Isal no.0071:441p, 2000.
[23] E. Gourdon, C.H. Lamarque, Energy pumping for a larger span of energy, *Journal of Sound and Vibration* 285 (3) (2005) 711–720.
[24] S. Mallat, A theory for multiresolution signal decomposition: the wavelet representation, *IEEE Transactions on Pattern Analysis and Machine Intelligence* 11 (1989) 674–693.
[25] I. Daubechies, Orthogonal bases of compactly supported wavelets, *Communication on Pure and Applied Mathematics XLV* (1998) 909–996.
[26] A.F. Vakakis, Inducing passive nonlinear energy sinks in vibrating systems, *ASME Transactions, Journal of Vibration and Acoustics* 123 (3) (2001) 324–332.